Aus dem

Department for Experimental Pathology, Mayo Clinic

Prof. Viji Shridhar, PhD

und

Aus der

Medizinischen Klinik und Poliklinik IV

Klinik der Universität München

Direktor: Prof. Dr. Martin Reinke

The effects of the heparan mimetic PG545 on cell growth and chemoresistance in Endometrial Cancer

Dissertation

zum Erwerb des Doktorgrades der Medizin

an der Medizinischen Fakultät

der Ludwig-Maximilians-Universität zu München

vorgelegt von

Robert Maximilian Hoffmann

aus Nürnberg

Jahr

2024

Mit Genehmigung der Medizinischen Fakultät

der Universität München

Berichterstatter:	Prof. Dr. Ralf Schmidmaier
Mitberichterstatter:	Prof. Dr. Nadia Harbeck
	PD Dr. Barbara Mayer
Dekan:	Prof. Dr. med. Thomas Gudermann
Tag der mündlichen Prüfung:	11.07.2024

Für Mollie und meine Familie

Table of contents

Abbreviations

AKT	Protein Kinase B
Annexin V-FITC	Annexin V- Fluorescein isothiocyanate
BiP	Binding Immunoglobulin Protein
BSA	Bovine Serum Albumin
CD31	Cluster of Differentiation 31
CFA	Colony Formation Assay
CHOP	CCAAT-enhancer-binding Protein Homologous Protein
CI	Combination Index
CPT	Cisplatin
CQ	Chloroquine
CTCF	Corrected Total Cell Fluorescence
DAPI	4′,6-diamidino-2-phenylindole
DMEM	Dulbecco's Modified Eagle Medium
DMSO	Dimethyl Sulfoxide
DPX	Dapoxyl Dye
EC	Endometrial Cancer
ECM	extracellular matrix
ER	Endoplasmatic Reticulum
ERBB2	Erb-B2 Receptor Tyrosine Kinase 2
FGF2	Fibroblast Growth Factor 2
FIA	Fluorometric Invasion Assay
Fig.	Figure

GADD153	Growth Arrest and DNA Damage 153 (also known as CHOP)
GAPDH	Glyceraldehyde-3-phosphate dehydrogenase
GF	Growth Factor
GFP	Green Fluorescent Protein
Grp78	Glucose Regulated Protein 78 (also known as BiP)
HB-EGF	Heparin-binding Epithelial Growth Factor
HB-GF	Heparin-binding Growth Factor
HBSS	Hank's Balanced Salt Solution
HER2	Human Epidermal Growth Factor Receptor 2
HEPES	4-(2-Hydroxyethyl)piperazine-1-ethanesulfonic acid sodium salt
HGF	Hepatocyte Growth Factor
HSPE	Heparanase
HSPG	Heparan sulfate proteoglycans
IACUC	Institutional Animal Care and Use Committee
IC50	Half-maximal Inhibitory Concentration
IFN-γ	Interferon- Gamma
IgG	Immunoglobulin G
iMVD	Intratumoral Microvessel Density
IRE1α	Inositol-requiring Enzyme α
K-Ras	Kirsten-Rat-Sarcoma Virus Oncogene

LC3BI/II	Microtubule-associated protein 1A/1B-light chain 3 I/II
MAPK	Mitogen-activated Protein Kinase Kinase
MEK	same as MAPK
mTOR	Mammalian Target of Rapamycin
MTT	[3-(4,5-dimethylthiazol-2-yl)-2,5-diphenyltetrazolium bromide]
PARP	Poly [ADP-ribose] polymerase 1
PBS	phosphate buffer saline
PCNA	Proliferating cell nuclear antigen
PDGF	Platelet-derived Growth Factor
pERK	Phosphorylated extracellular signal-regulated kinase
PERK	Protein kinase R (PKR)-like endoplasmic reticulum kinase
PI	Propidium Iodide
PI3K	Phosphoinositide 3-kinase
PTEN	Phosphatase and Tensin Homolog
PTX	Paclitaxel
PARP	poly (ADP-ribose) polymerase
CQ	Chloroquine
RTK	Receptor Tyrosine Kinase
S.D.	Standard Deviation
SDS	Sodium Dodecyl sulfate
TBST	Tris Buffered Saline with Tween
UPR	Unfolded protein response
VEGF	Vascular endothelial Growth Factor

VEGFR2	Vascular Endothelial Growth Factor Receptor 2

Figures

Tables

1. Introduction

Endometrial Cancer (EC) is the most common gynecologic malignancy worldwide. Over the last decade incidence and fatalities have been rising continually bringing EC into the spotlight as a major public health concern [1], [2]. EC accounted for 12,650 deaths in the United States in 2020 a 15% increase from 2012 [3]. The cases of Endometrial Cancer likely continue to rise as risk factors for its development such as obesity and advanced age become more prevalent in Western society [4].

Endometrial Cancer commonly is detected at an early stage with abnormal vaginal bleeding or menstrual irregularities making a timely diagnosis in most cases possible. In early stages Endometrial cancer can be cured with resection, radiation and hormonal therapy with 5-year survival rates reaching up to 90%[5]–[7]. A subset of patients presents with advanced stage disease and an often-underlying aggressive histologic phenotype resulting in poor overall survival [8]. Aggressive phenotype and advanced stage disease necessitate the addition of chemotherapy therapy next to surgery. Several studies have shown that systemic chemotherapy reduces disease recurrence and prolongs overall survival in advanced endometrial cancer [8]. The most frequently used chemotherapeutic regimen consists of a combination of platin- and a taxol-based agents. This combination has been shown to results in an overall response in advanced endometrial cancer of up to 50% [9]. Despite progresses in the usage of chemotherapy over the last two decades, chemotherapy is associated with significant side effects impacting the quality of life for patients and leading to significant morbidity in endometrial cancer patients [10]. Moreover, repetitive chemotherapy cycles have been shown to induce chemoresistance in endometrial cancer cells [11]. For patients with systemic disease chemoresistance is a key driver of disease progress and mortality [12]. Hence, identifying escape pathways and targeting

mechanism mediating chemoresistance is essential to further improve care for patients with EC. Several biochemical pathways facilitating chemoresistance have emerged as potential therapeutic targets in endometrial cancer opening promising avenues for EC treatment.

The biology of Endometrial Cancer is complex and the disease itself is extremely heterogenous [13]. Pathologically EC is commonly classified into two subtypes type I and type II endometrial cancer [14]. Type I Endometrial Cancer is by far more common representing approximately 80% - 85% of EC cases. Its histology typically shows an endometrioid appearance [15]. Type I is typically associated with a less aggressive slower growing phenotype which is often only minimally invasive and thought to be estrogen dependent [16]. A clear molecular distinction can be made between both subtypes. [17] PTEN loss, K-Ras mutation and microsatellite instability are the most commonly observed genomic aberrations in Type I [18]–[20]. Type II, on the other hand, has histologically often a clear cell or serous appearance and appears less differentiated [21]. Type II is less common than type I while accounting for more deaths highlighting its clinical aggressiveness. It often presents at a later stage and is significantly associated with poorer prognosis compared to type I EC. Genetically, alterations in p53, p16, HER2 and E-Cadherin are observed in type II EC [22]. Nevertheless, distinct molecular overlap exists between both subtypes. For example, increased expression of various heparin-binding growth factors (HB-GFs) including FGF, HGF, VEGF and HB-EGF and their respective receptors, tyrosine kinases embedded in the cellular membrane, are known to promote angiogenesis and are associated with worse survival in EC [23], [24]. Therefore, growth factors and their cognate receptors emerged as promising therapeutic target in Endometrial Cancer research [25], [26].

Cells meticulously regulate their growth and division through tightly controlled signaling cascades. These are typically initiated by growth factors binding to receptor tyrosine kinases (RTKs). Overexpression or dysregulation of components of signaling pathways such as the RTK pathway has been described as one of the hallmarks of cancer [27]. By overriding regulating inhibitory signals and conferring a selective advantage to cancer cells aberrant RTK-signaling is a key driver of tumorigenesis in many cancers. In EC, various growth factors and RTK signaling have been linked to tumorigenesis, angiogenesis, and metastasis [28]. Furthermore, growth factors, particularly involving RTK pathways, significantly contribute to chemoresistance in EC [29]. Loss of PTEN, a tumor suppressor gene or inhibitor in the growth promoting PI3K signaling pathway is by far the most observed mutation in endometrial cancer. Noted in up to 91% of EC cases, PTEN loss results in subsequent upregulation of PI3K, a intracellular signal transducer activated via tyrosine kinases and their ligands, most notably EGF, hEGF (HER2 ligand) and FGF [30], [31]. Uninhibited PI3K activation leads to increased levels of phosphorylated AKT in the cancer cell. Once phosphorylated AKT acts as a mediator of chemoresistance via mitochondrial apoptotic pathways and upregulation of mTOR [32], [33]. Mutations in AKT mediated signaling pathway have been shown to be linked to chemoresistance of EC cells to the most frequently used chemotherapeutic agents in EC: Cisplatin, Paclitaxel and Doxorubicin[32], [34], [35]. Additionally, RTK pathways exhibit significant interdependence and crosstalk, hence dysregulation in one lead to activation in others such as the Ras-MEK-MAPK-ERK (or simply MAPK-pathway) further promoting chemoresistance when pAKT is upregulated [36]. The MAPK-pathway is another tyrosine kinase induced pathway promoting cell proliferation and tumorigenesis. With regards to chemoresistance it has been shown to attenuate effects of chemotherapy

in EC through atypical activation of ERK1 and mediating dysregulated signaling [37]–[39]. Simultaneous mutations in the pathway appear to particularly facilitate chemoresistance to platin agents [36].

Based on the link to tumor biology and chemoresistance described above main therapeutic targets in recent or ongoing clinical trials have been the by PTEN loss upregulated PI3K/mTOR/AKT pathway or aforementioned growth factors and their associated receptor [29] . Hopes for targeting these pathways are to either inhibit EC growth or to sensitize endometrial cancer cells to cytotoxic therapy. Despite PI3K pathway mutations being the most common associated alteration in EC, the use of approved or experimental mTOR inhibitors has been overall disappointing [40]. Upregulation of compensatory feedback loops such as the MAPK, AKT and RAS/RAF/MEK pathways have been discussed as potential escape mechanisms as these same pathways are frequently altered in EC [31], [41], [42]. HER2, a tyrosine kinase receptor, appears to be upregulated in 17-33% of Endometrial cancer [43]. Signal induction via tyrosine kinase receptor HER2 (ERBB2) results in activation of PI3K and MAPK pathways. Both specific inhibition of HER2 as well as non-specific inhibition of Tyrosine kinases via EGFR inhibitors have been trialed in EC [44]–[46]. Results are mixed as no significant response rate was observed in type I EC, but progression free survival improved in serous uterine carcinoma [47]. While in EC type 1 response was not correlating with HER2 or EGFR status of the tumors, HER2 status was a positive predictor of therapeutic response in serous EC. This highlights how complex and unpredictable the interaction between biology and targeting of single molecular targets is. Lastly, non-EGFR tyrosine kinase inhibitors were used, targeting cascades activated by VEGF, FGF, PDGF. Again, with similar modest outcomes despite using agents such as sunitinib which multitargets tyrosine kinase receptors

including VEGF1,2,3 and PDGF [44], [48]. In summary the outcome of these trials brings into question whether therapeutic targeting of single tumor promoting pathways or mutations can lead to substantial clinical responses in Endometrial Cancer. Biological Heterogeneity and distinct resistance mechanisms in EC may represent obstacles too complex to overcome for single pathway targeting [49]. An alternative approach in EC therapy may represent to use agents or combinations of drugs, which target various tumor promoting mechanisms simultaneously, targeting several pathways at the same time by doing so potentially inhibit EC more effectively than single pathway agents are able to.

Heparan sulfate (HS) proteoglycans (HSPG) have been described to play a role in various aspects of tumorigenesis [50]. Through their covalently bound heparan sulfate chain HSPGs structure and regulate the extracellular matrix (ECM). HSPGs bind via their HS portion many ligands in the extracellular space including aforementioned heparin binding growth factors [51]. Heparanase, a β-endoglucorinadase located intra- and extracellularly, enzymatically cleaves HSPGs releasing the heparin-binding growth factors attached to the proteoglycans [52]. Through its enzymatic activity it releases the ligands bound to HSPGs such as hEGF, FGF, VEGF and HB-EGF thereby supporting proliferation and vascular formation of the tumor in its surrounding tissues. Reversely, when heparanase is silenced tumors demonstrate reduced angiogenic and proliferative capabilities [53]. Furthermore, by degrading HSPGs, heparanase breaks down the ECM, reducing structural barriers surrounding the tumor and leading to further infiltration and seeding of cancer cells in the adjacent tissue [54]. HSPGs can also be found on the tumor cell surfaces [55]. Perlecan, a proteoglycan binding VEGF, is cleaved by heparanase releasing VEGF for further vascularization [56]. Syndecan-1, another transmembrane proteoglycan,

has been shown to be shed by heparanase. The shed form of syndecan then stimulates VEGFR2 receptors and downstream signaling molecules including PI3K, AKT isoforms and ERK [57]. Heparanase not only promotes tumor invasion extracellularly, it has also been linked intracellularly to tumor-promoting features. Activation of EGFR has been shown to promote nucleolar translocation of heparanase inducing topoisomerase I transcription and therapy supporting cell proliferation [58]. In Endometrial Cancer heparanase is found to be significantly increased [59]. Specimen of endometrial cancer with increased heparanase expression were more likely to penetrate the myometrium deeper and are also more likely to have infiltrated lymph nodes [60]. Increased heparanse expression has been linked to less differentiated, generally more aggressive histological subtype [61]. Certain HSPGs, i.e. syndecan-1 are downregulated in EC and other cancers [60]. Normally they act as messenger for differentiation, as barrier to the epithelial-mesenchymal transition, a pivotal step for metastasis in cancer[62], [63]. In EC they are commonly altered on tumor cells, indicating a more profound role of the heparanase-HSPG system in tumorigenesis in EC [64]. As demonstrated through its multifaceted activity in modulating the tumor's microenvironment this system plays a potentially vital role in carcinogenesis of EC and other cancers [65]. Therefore, inhibiting the interplay between heparanase and HSPGs and the resulting effects on ECM, growth factors and intracellular cascades appears to be a promising multitargeting approach in cancer therapy [66].

Several compounds have been described to inhibit heparanase. One of them is PG545 is a fully sulfated heparan mimetic. It is currently under investigation in a Phase I clinical trial [67]. It was selected among a group of pharmacologic candidates for its potent inhibition of heparin binding growth factors like VGEF and FGF [68]. It also binds and subsequently inhibits heparanase. PG545 is a fully sulfated

oligosaccharide resembling the anticoagulant heparin. Through a functional attachment of cholestanol glycol to the saccharide portion, PG545 is able to prevent enzymatic activity of heparanase without significant anticoaguable side effects [66]. By targeting the heparanase-HSPG system PG 545 has been shown to inhibit proliferation, angiogenesis and prevent metastasis in preclinical models [69]. Our group demonstrated that PG545 effectively blocks HBGF signaling in ovarian cancer [70]. Synergistic effects with cisplatin and paclitaxel were demonstrated in preclinical models highlighting the attenuating effects of PG545 to chemoresistance. These effects were demonstrated in athymic as well as immunocompetent mouse models [70]. By blocking HBG PG545 induces DNA single- and double- strand breaks and inhibits homologous repair, potentiating the effect of poly (ADP-ribose) polymerase (PARP) inhibitors) and chemotherapy in ovarian cancer [71]. We demonstrated that VEGF levels in patients treated with PG545 were increased after drug administration, suggesting reduced bioavailability of VEGF in patients [70]. In preclinical pancreatic tumor studies, similar synergistic effects were observed between PG545 and chemotherapeutic agents [72], [73]. Furthermore, PG545 administration effectively inhibits Wnt and hence Beta-Catenin activation, another signaling cascade impacted by heparanase. PG545 not only inhibits heparanase and HS-mediated growth factor signaling functions, it also has been recently described as an immunomodulator by activating NK cells via dendritic cells [74]. In a phase 1B trial, PG545 administration resulted in increased levels of TNF, IFN-γ and other immune cytokines, which correlates with the immunostimulatory effects described in *in vitro* models [67]. Lastly, PG545 was shown to inhibit autophagy via inhibition of heparanase in cancer cells [75].

Autophagy is a catabolic process serving cell homeostasis by degrading intracellular material [76]. Autophagy is upregulated in conditions of nutritional starvation to preserve cellular functioning. By maintaining homeostasis in unfavorable conditions, autophagy is linked to cell survival and chemoresistance in cancer cells [77]. Nevertheless, autophagy is viewed as “double edged sword”, as early tumor development seems to be inhibited by autophagy [78]. Furthermore, excessive induction of authophagic processes has been shown to overwhelm cell homeostasis and induce autophagic cell death [79]. Hence autophagy has been linked to both carcinogenesis and antitumor effects. The relationship between the chemo sensitizing properties of PG545 and induction of autophagy via heparanase-HSPG has not yet been characterized.

In summary PG545 shows several antitumor activities along several tumorigenic pathways. Its multitargeting properties, particularly along growth factor induced tyrosine kinase activation, make it a promising candidate for treating endometrial cancer. This notion is further supported by its strong antitumor effects in ovarian cancer, which demonstrates genotypic similarities when compared to aggressive type II endometrial cancer. PG545 also shows synergistic properties with chemotherapy demonstrated across various tumor models. Given the frequent failure rate of chemotherapy in EC, adjuncts to cytotoxic therapy are urgently needed. Therefore, our study aims to investigate PG545 in endometrial cancer and its effects to proliferation and chemoresistance in endometrial cancer.

The objective of this study was to evaluate the efficacy of PG545 alone and in combination with the chemotherapeutic agents cisplatin and paclitaxel in both type I and type II endometrial cancer. Additionally, to cell culture studies, we also used a mouse xenograft model to describe the effects of PG545 *in vivo*. To my knowledge

this is the first study to describe the effects of PG545 or any heparan mimetic in endometrial cancer. By using a total of four different cell lines consisting of both type I and II we try to account for the disease's known heterogeneity. Mechanistically this study aims to describe PG545 downstream effects on growth factor signaling in type and type II EC. As highlighted above PG545 has been shown to exhibit significant chemosensitizing properties in various carcinomas cell lines. Autophagy is a known mediator of chemoresistance, therefore we wanted to investigate the effects of PG545 on autophagy in EC. A subsequent hypothesis of ER stress linking autophagy and chemosensitivity arose when autophagy was observed, despite PG545's chemosensitizing properties. Therefore, additional experiments were conducted to study ER stress response to PG545 treatment.

Results listed in chapter 3.1. – 3.13 of this dissertation are previously published in *"Sulfated glycolipid PG545 induces endoplasmic reticulum stress and augments autophagic flux by enhancing anticancer chemotherapy efficacy in endometrial cancer*" by *R. Hoffmann et al*, Biochemical Pharmacology, August 2020, https://doi.org/10.1016/j.bcp.2020.114003 [80]. The experiments demonstrated in Figure 12 were conducted by Dr. Bhattarchayan. I provided input on cell handling and drug mixing.

2. Materials and Methods

5.1. Chemical reagents

Zucero Therapeutics (Melbourne, Australia) kindly supplied PG545. PG545 was refrigerated in powder form and freshly mixed with phosphate buffer saline (PBS, Gibco, USA) shortly before each *in vitro* or *in vivo* application. Cisplatin was acquired from EMD Millipore (Calbiochem, Millipore, Billerica, MA) and stored accordingly in 15-25 Celsius degree protected from light. Paclitaxel (30 mg/5mL) from Hospira (Lake Forest, IL) was stored at room temperature and under protection from light as well. Similarly, to PG545 both compounds were freshly mixed before each *in vitro* or *in vivo* administration. Both compounds were mixed in phosphate buffer saline (PBS, Gibco, USA). We obtained primary antibodies directed against total- and phosphor- ERK, total- and phosphor-Akt, LC3BI/II, CHOP, Bip, GAPDH, IRE1α, from Cell Signaling Technology (Danvers, MA). Antibodies were supplied and stored in 4-(2-Hydroxyethyl)piperazine-1-ethanesulfonic acid sodium salt (HEPES; pH 7.5), 150 mM sodium chloride, 100 µg/ml Bovine Serum Albumin (BSA) and 50% glycerol at –20°C. Antibodies were mixed prior to application in 1:1000 dilution with 5% Bovine Serum Albumin in TBST 1x as per Cell Signaling Technology protocol. Secondary antibodies of mouse and rabbit IgG were also bought from Cell Signaling Technology. Primary antibodies against PCNA, Calnexin and p62 were obtained from Santa Cruz (Santa Cruz, CA). Antibodies were obtained in 200 µg IgG_{2a} kappa light chain in 1.0 ml of PBS with < 0.1% sodium azide and 0.1% gelatin and was stored in 4°C. Antibodies were mixed according to protocol in 1:1000 dilution with 5% Bovine Serum Albumin in Tris Buffered Saline with Tween (TBST) 1x prior to application.

5.2. Cell lines

We used four different endometrial cancer cell lines *in vitro*, each representing a pathohistological subtype of endometrial cancer [81]. The four cell lines are Ishikawa, RL95-2, Hec1B and ARK2 cells. Ishikawa cells are described as slower growing, more differentiated and endometrioid in appearance [82]. RL95-2 are less differentiated and tend to be more aggressive [83]. Hec1B cells are referred to as endometrioid type I cells which show significant cisplatin resistance [84]. ARK2 cells are serous carcinoma cells [85]. Dr. Paul Goodfellow from Washington University in St Louis kindly provided our laboratory with Ishikawa and RL95-2 cells. The serous carcinoma ARK2 cells were generously supplied by Professor Shi-Wen Jiang (formerly affiliated with Dr. Karl Podratz, Mayo Clinic, Rochester, MN). The platin resistant Hec1B cells were acquired from ATCC (American Type Culture Collection, Manassas, VA). DMEM/F12 media (Thermo Fisher, Waltham, MA), was used for incubation of Hec1B, ARK2 and RL95-2. Ishikawa cells were cultured in DMEM media (Thermo Fisher, Waltham, MA). 10% FBS (Fetal Bovine Serum) was added in conjunction with an antibiotic-antimycotic solution. All cell lines were furthermore tested for viral colonization by the Mayo Clinic Microbiology Laboratory (Rochester, MN). Cells were kept in an incubation chamber providing humidified atmosphere of 37ºC with 5% CO_2. Cells were regularly split to avoid overcrowding. Prior to each experiment cells were harvested when approximately 80% to 90% confluent. Cells were washed with PBS, then incubated with Trypsin 0.05% (Thermo Fisher, Waltham, MA) for ca. 1-2 min to promote cell detachment. Cells were then harvested in cell media and counted under a microscope with a Neubauer chamber. If not used for immediate experiments or for ongoing cell culturing cells were cooled down to -80ºC in culture media and 10% DMSO (Dimethyl Sulfoxide) and transferred to a liquid nitrogen tank after 24 hours.

5.3. Colony Formation Assay (CFA)

For our Colony Formation Assay we plated $1X10^3$ cells in round 6-well plates with 3.5 cm diameter (Thermo Fisher, Waltham, MA) with 1.5 mL culture medium. Cells were then incubated for 24 hours. Cell attachment and viability were assured prior to adding PG545. PG545 was then added with new cell media in triple replicates resulting in concentrations of 2.5, 5, 10, 20 and 40 µM. The Solution was removed after 24 hours and replaced with cell media. Colonies were incubated for another 5 days. Media was then removed, and colonies were subsequently fixated with methanol (Thermo Fisher, Waltham, MA). We used 0.5% crystal violet (Millipore-Sigma USA) to stain each colony [86]. Colony numbers were measured using Quantity One (Bio-Rad, California, USA) software. Each Assay was repeated at least three times.

5.4. Cell Viability Assay

In order to assess in vitro cell viability and cytotoxicity of various drug regimen MTT [3-(4,5-dimethylthiazol-2-yl)-2,5-diphenyltetrazolium bromide] (Millipore-Sigma USA) assay was applied. 5 $X10^3$ cells were added per well of a 96 well plate (Thermo Fisher, Waltham, MA). After a 24-hour incubation period, media with indicated drug concentrations of PG545, Cisplatin and paclitaxel were added. Cells were then incubated for 48 hours unless indicated otherwise. Each drug concentration was applied in five wells. After the incubation period 20 µl of MTT was pipetted into the drug containing media. After four hours the solution was carefully removed with a glass pipette under suction. 200 µL Dimethyl Sulfoxide (DMSO) were then applied to each well. After a brief incubation period of three to five minutes plates were then placed in a microplate reader. Absorbance was measured by a spectrophotometer (Fischer Scientific, Waltham, MA) at 490 nm wavelength for each well. Absorbance values were

then normalized to each group's control wells. Each experiment was replicated at least 3 times.

5.5. Synergy calculations

The readings from the spectrophotometer were imported into the analysis program Prism (GraphPad Software, La Jolla, CA) and CalcuSyn (Biosoft, USA). The half-maximal Inhibitory Concentrations (IC50) were then determined for all drugs and cell lines used in synergy studies. Increasing concentrations of PG545, cisplatin, paclitaxel was added for 48 hours and assessed via MTT assay. Out of these data sets, IC50 values were determined through a dose-response curve calculated by Prism software [87].

The IC50 concentrations were then used to assess synergy between PG 545 and the chemotherapeutic agents Cisplatin and Paclitaxel according to the Chou-Talalay method [88]. We conducted MTT assays with a constant ratio (multiples of IC_{50}: $IC_{50\ ratios}$) between PG545 and each chemotherapeutic agent. Combination Index (CI) values were then determined via a Chou-Martin plot calculated by the CalcuSyn software. 95% confidence intervals were also calculated. The Combination Index (CI) is used to classify drug interactions into synergy (CI ≤ 0.9), addition (CI >0.9; ≤ 1.1) or antagonism (CI > 1.1). Synergy can be further described as strong with CI values ranging from 0.3-0.7, as moderate when CI values ranged 0,7 – 0.85 and as weak if CI values range from 0.85 – 0.9 [87].

5.6. Western Blots

Western Blots were performed as previously described [89]. Western blot experiments were conducted from 1 x 10^6 cells growing in 60 mm petri dishes for 24 hours (Fisher Scientific, Waltham, MA) unless otherwise indicated in the specific

method sections. Cells were incubated with growth factor, PG545 and melatonin with each time course being indicated in the result section. Lysis buffer containing a protease inhibitor (Roche, Indianapolis, IN) and containing freshly added 2.5% β-mercaptoethanol, was added and cells were scraped off. Cells were sonicated for protein extraction with Ultrasonic Processor (Cole-Palmer, Vernon Hills, IL) at 40% output for 10 seconds, and boiled for 5 minutes. Cells were then cooled on ice and centrifuged. Protein concentration was determined for each sample via Bradford Assay (BioRad, Hercules, CA). Whole-cell lysates containing equal amounts of protein were separated via gel electrophoresis using polyacrylamide gels (Novex, Thermo Fischer) in buffer with SDS (Sodium dodecyl sulfate). Proteins were transferred to nitrocellulose membrane via electroblotting (Transfer cassettes from Bio-Rad, CA). Membranes were blocked with 3% Fetal Bovine Serum to prevent non-specific cross reaction. Incubation period for 24 hours with primary antibody solution (1:1000 dilution) was followed by secondary mouse or rabbit antibody incubation (Santa Cruz, CA) for one hour. Image was obtained via LI-COR Imaging system (LI-COR, NE). Every western blot was performed at least three times, and a representative blot image was shown in the figures. The densitometric quantification of the western blots was shown in the figures.

5.7. Migration (Wound Scratch) Assay

1×10^5 Cells were plated on 12-well plates with a culture area of 3.85 cm^2. At 80%-90% confluency cells were scratched with a 200 µl pipette tip. The medium was then changed to not containing any serum. Cells were incubated with FBS equal to 10% of the volume, HB-EGF resulting in a concentration of 50 ng/mL and FGF-2 resulting in a concentration of 10 ng/mL (all Gibco, USA). Treatment groups received

10 μM of PG545 and were incubated for 24 hours. Pictures were obtained at 10 x magnification. The area of migration was then assessed via ImageJ software.

5.8. Invasion Assay

We used 1× 10^5 Hec1B and ARK2 cells (1× 10^5) per chamber of a 12-well plate containing Fluorimetric Invasion Assay (FIA) chamber (Corning, NY). Each well consists of two chambers separated by a Matrigel layer. The inner compartment contained medium lacking any growth factors, while the outer compartment contained FBS equal to 10% of the volume or HB-EGF in 50 ng/mL concentration acting as chemoattractant. PG545 was added in a concentration of 10 μM to the treatment groups. Cells were then incubated for 48 hours. After fixation cells were stained with Coomassie Staining (BioRad, CA). The cells were then counted per well in replicates of three via Quantity One (Bio-Rad, CA) software to assess invasion of the outer surface membrane.

5.9. Apoptosis Staining via Annexin V/PI double staining

We plated 1x10^6 cell on 60 mm petri dishes and incubated them for 24 hours. When confluency of 80%-90% was achieved we treated samples for 24 hours with 20 μM PG545 and/or 20 μM cisplatin and 50 nM paclitaxel. We harvested the cells and washed them 3x with PBS to remove any residual media or treatment agents. The EC cells were stained with an Apoptosis detection kit (Roche, USA) and labeled with Annexin V-FITC and Propidium Iodide according to the instructions by the manufacturer. Cells were then quantified by FACSCalibur (Becton Dickinson, USA) measuring Annexin V-FITC and PI-positive cells. All experiments were repeated at least three times.

5.10. Xenograft models

Prior to all *in vivo* experiments approval by the Institutional Animal Care and Use Committee of Mayo Clinic (IACUC) was obtained. We generated Hec1B (type I EC) and ARK2 (type II EC) xenograft models by injecting $2.5x10^6$ Hec1B and $1.5x10^6$ ARK2 subcutaneously in 6–8-week-old female nude, athymic mice obtained from Harlan Laboratories (Indianapolis, IN). Based on prior studies with HEC 1B and ARK2 cells we decided to reduce the number of cells in the ARK2 xenograft model due to the aggressive behavior of these cells *in vivo*. Prior to injection cells were cultured to 80%-90% confluency. After counting the appropriate number of cells, they were suspended in 0.2 mL of PBS and subsequently injected into the right flank of each mouse. Tumor progress was monitored every other day. Once all tumors reached a minimal volume of 3 mm x 3mm x 3mm, all mice were randomly assigned into four groups of ten animals each. Tumor size was assessed every four days using a caliber. The tumor size was approximated based on an assumed ellipsoid volume via the following formula: volume=π /6 x length x $width^2$. Treatment was initiated in both xenograft models 7 days after inoculation. The event criteria for the survival study were defined according to IACUC protocols as follows: 1. Ulceration of the tumor site 2. Tumor is measuring more than 1200 mm^3 3. Any tumor diameter exceeding 20 mm. 4. Loss of weight >10% from baseline weight. The study concluded on day 72 after inoculation when no further endpoint criterion was met at the time.

Both Hec1B and ARK2 xenograft models were divided into the following four treatment groups: Control, 200 µl of PBS were administered every third day as placebo. Chemotherapy: The regimen consisting of (4mg/kg) Cisplatin plus (16 mg/kg) paclitaxel was given via intraperitoneal injection on days 7, 12, and 16 as previously described by our group in [73] PG545: 20 mg/kg of PG545 was administered every

third day until the conclusion of the study [70], [87]. Combination: PG545 with equivalent dosing from the single treatment group (20 mg/kg) was combined with the dosing regimen form the chemotherapy group (**Figure 1**).

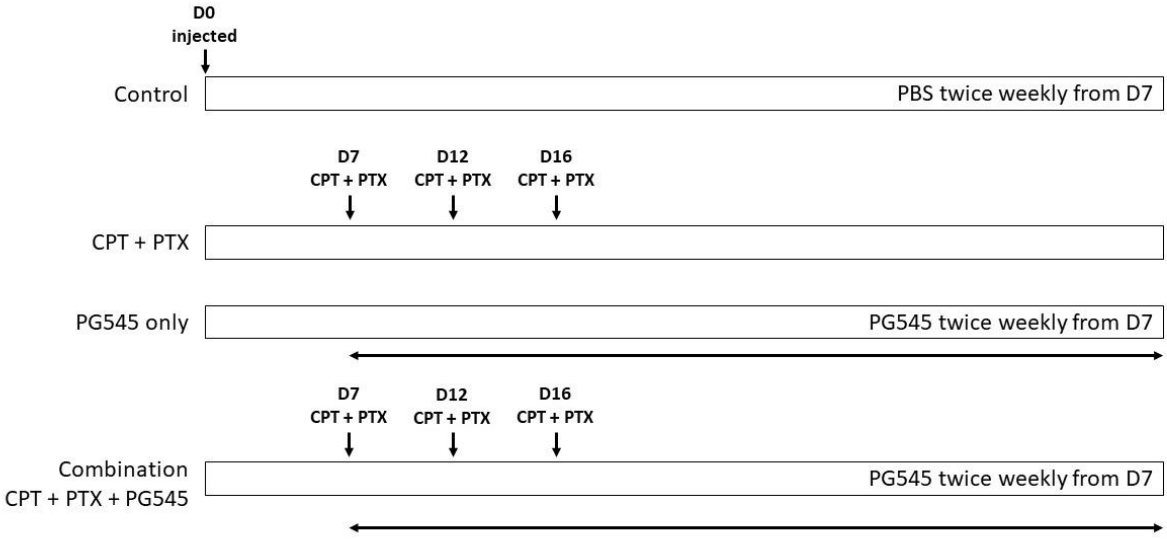

Figure 1: Visualization of the treatment regimen used for Hec1B and ARK2 xenograft models.

5.11. Immunohistochemistry

The immunohistochemistry staining for all xenograft tumors was conducted by the Pathology Research Core Laboratory at Mayo Clinic, Rochester, MN, following the standard protocol. Tissue sections embedded in paraffin were specifically stained for Ki67 and CD31 and subsequently analyzed. CD31, a marker indicative of vascular endothelium, was utilized to evaluate intratumoral microvessel density (iMVD). After scanning with 20 x magnification the entire tumor section representative areas, numbering three per tumor, were identified, and captured using a Zeiss LSM 510

microscope. Microvessel structures were then quantified, and comparisons were made among the various treatment groups [90]. The assessment of Ki67 staining employed the freely available ImageJ Add-on ImmunoRatio [91]. Pictures were obtained using 40x magnification. For every imaging session we also obtained a blank image to allow the software to correct background image color and illumination. With the Camera Adjustment Wizard, included in the ImmunoRatio software color deconvolution is performed separating diaminobenzidine and hematoxylin both stains of the immunohistochemistry. One separated the software calculates with a watershed algorithm the hematoxylin-stained nuclei able to determine the ratio of ki67 positive nuclei.

5.12. Cyto-ID staining and detection of autophagosomes

We plated 1 x 10^4 Hec1B and ARK2 cells in 4-well chambered slides (BD Falcon, USA) and treated with 0 µM, 10 µM or 20 µM of PG545. After 24 hours, cells were washed 2x with PBS and a Cyto-ID autophagy detection kit (Enzo Life Sciences) was used to detect autophagic vesicles [92]. In brief cells are being incubated for 30 min with the fluorescent Cyto-ID dye, a marker specifically attaching to autophagy compartments in the cells. In order to identify nuclei cells were with 4′,6-diamidino-2-phenylindole (DAPI) which was included in the detection kit. Cells were then washed x2 with PBS to remove any residual dye. Images were taken with a Zeiss LSM 510 microscope. Quantification of Corrected Total Cell Fluorescence (CTCF) was assessed as integrated density-(area of selected cell x mean fluorescence of background reading) as average of 25 cells via ImageJ software.

5.13. Quantification of autophagic flux by monomeric (m) Cherry-GFP-LC3 transfection and confocal microscopy

We plated 1 x 10^4 Hec1B in 4-well chambered slides. The cells were transfected for 48 hours with mCherry-GFP-LC3B plasmid which was kindly provided by Dr. Daniel Billadeu (Mayo Clinic, Rochester, MN) [93]After x2 wash with PBS, DMEM/F12 with 10%FBS was reapplied and the cells were treated with 0 µM, 10 µM or 20 µM of PG545 with or without 50 nM of the autophagic flux inhibitor bafilomycin [94]. Cells were then washed three times and fixated. Confocal microscopy was performed with a Zeiss LSM 510 microscope. Confocal microscopy was performed to visualize the green-fluorescent labelled GFP and red-fluorescent labelled mCherry proteins. Changes in the ratio of these markers represent autophagic flux. Quantification was performed with ImageJ software.

5.14. Detection of ER activity by ER tracker Blue-White DPX staining

ER activity and stress were assessed by fluorescence microscopy using an ER-tracker blue/white DPX stain [95]. Hec1B and ARK2 cells (5×10^3) were plated in 8 chambered polystyrene culture slides (BD Falcon, USA) per well in DMEM/F12 medium with 10% FBS. After 24 hours, media was removed and with 1x HBSS (Gibco, USA) with Mg^{++} (0.10 gm/L) and Ca^{++} (0.14 gm/L) substituted. PG545 with a concentration of 20 µM was added to all treatment groups. ER activity was investigated in a time-dependent manner. When the predetermined time point was reached the cells were x2 washed with 1x HBSS. ER-Tracker Blue-White DPX (Thermo Fisher, Waltham, MA) staining (500 nM) was administered together with the 1x HBSS Magnesium and Calcium solution and incubated for 30 mins at 37 °C at 5% CO_2. Afterwards the solution containing the dye was removed and the cells were washed

again with 1x HBSS. Samples were then evaluated under an EVOS fluorescent microscope. CTCF was determined via ImageJ software.

5.15. Statistical Analysis

Results are shown as mean ± standard deviation (S.D.) of at least three independent experiments unless otherwise indicated. Graph Pad Prism software (San Diego, CA) was used for statistical analyses. CalcuSyn (BioSoft, USA) software was used for calculation of combination indices as outlined above. Differences between groups sets were analyzed via paired t-test. Survival data were analyzed by using Log-Rank tests based on Kaplan Meyer curves. P-values < 0.05 were considered significant unless determined otherwise.

5.16. Laboratory

All experiments were conducted in the laboratory facilities of the Department for Experimental Pathology at Mayo Clinic Rochester, MN, USA. Laboratory facilities were kindly provided by Professor Viji Shridhar. Supervision of all experiments was ensured by Doctor Debarshi Roy, Doctor Sayantani Bhattacharia and Professor Viji Shriddhar.

3. Results

6.1. PG545 inhibits downstream signaling of heparin-binding growth factors.

First, we established that the known mechanism of action by PG545 to block heparin-binding growth factor signaling, pertains in endometrial cancer cell lines. For this we treated Hec1B cells, starved for 12 hours in serum free media, supplemented only with 50 ng/mL of FGF2 with 10 μM PG545 from 10 – 60 minutes. Both phosphorylation of Akt at Ser473 and ERK at Thr 202/204 are markedly reduced (**Figure 2A**). The attenuation of the signaling is prominent at the 60-minute mark. We then treated ARK2 cells with the same concentration of PG545 in serum starved medium supplemented with 50 ng/mL of HB-EGF. Western blot in phosphorylation of both Akt Ser 473 and ERK Thr202/204 is downregulated prominently at the 10-minute and 30-minute time point returning to near baseline levels (**Figure 2B**). We have published this result in our report to the activity of PG545 in endometrial cancer [80].

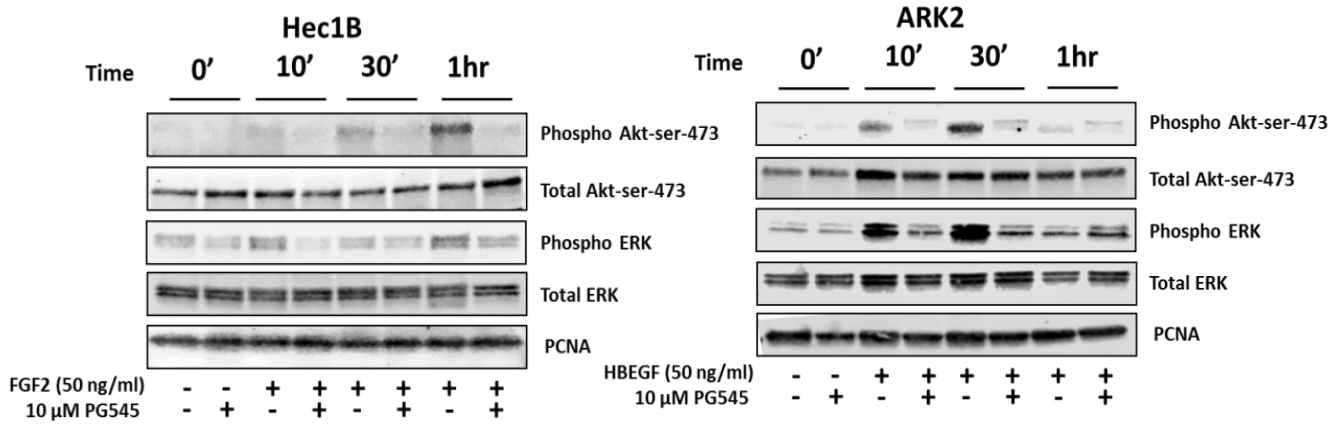

Figure 2: PG545 blocks downstream effects of HB-GFs. Hec1B and ARK2 cells were straved for 12 hours in serum-free media and then exposed to FGF2 (**A**) and HB-EGF (**B**) with and without 10 μM of PG545. Cells lysates were collected at 10, 30 and 60 minutes. Western blot demonstrated a reduction of phospho- Akt and phospho-ERK.

6.2. PG545 blocks growth factor mediated migration and invasion in Hec1B and ARK2 cells.

We investigated the effects of PG545 on in vitro cell migration assessed though wound scratch assay. After being scratched with the tip of a 200 µl pipette we exposed Hec1B and ARK2 cells to 10 µM of PG545 in media supplemented either with normal saline, FGF2, HB-EGF or 10%. We observed a significant reduction of the migrated area in all groups ($p<0.001$) when they were treated with PG545 (**Figure 3A and B**). The highest reduction compared to the untreated group was observed in Hec1B cells supplemented with HB-EGF (~60%) and ARK2 (~65%) cells supplemented with FGF2.

We used a Matrigel invasion assay to investigate the impact of PG545 of cell invasion in both cell lines (**Figure 3 C and D**). For this we added 10 µM of PG545 to the chamber with the chemoattractant, which was in our case media supplemented with normal saline,10% serum, FGF2 or HBEGF. ARK2 were found to be more invasive than HEC1B cells. In both cell lines invasion was markedly reduced when PG545 was added in both cell lines ($p<0.05$). This result was published in our report to the activity of PG545 in endometrial cancer [80]

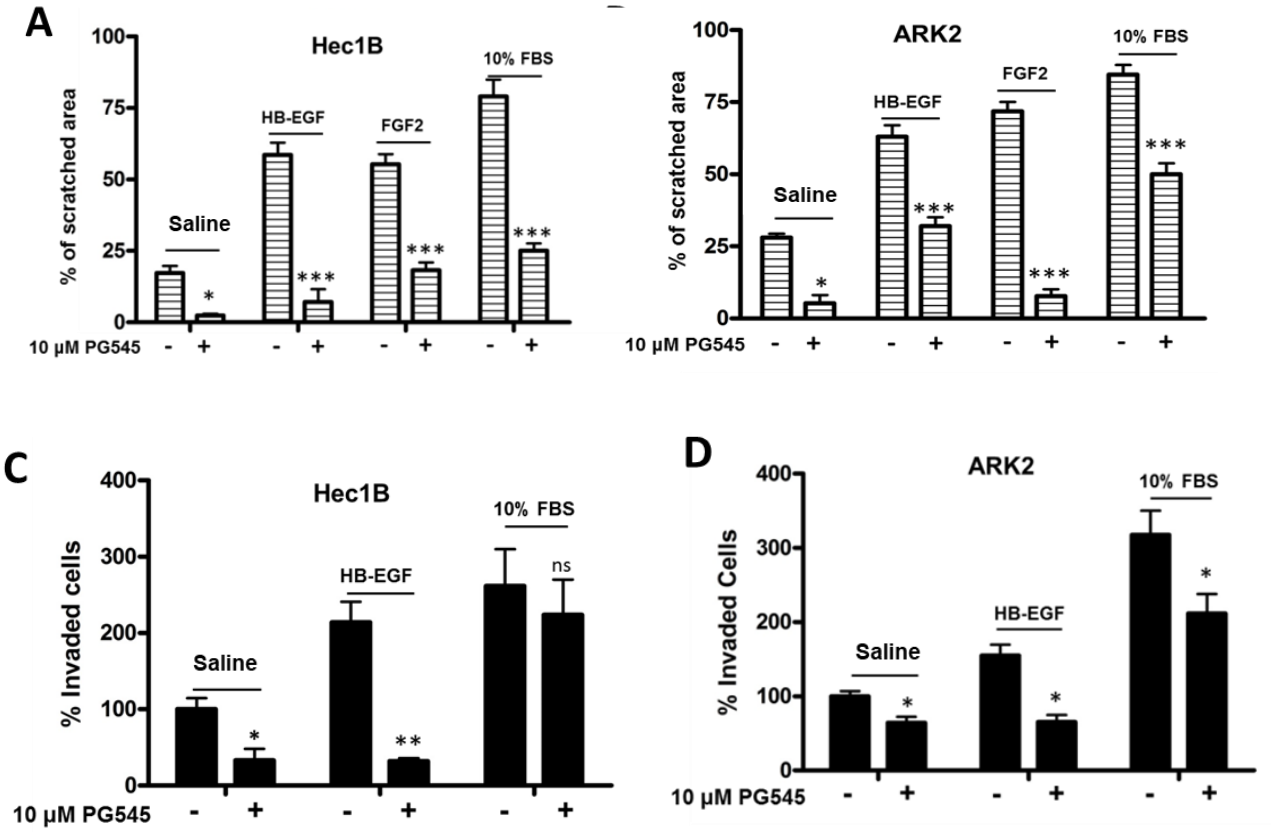

Figure 3: PG545 effectively blocks cell migration and invasion *in vitro*. Scratch assay assessed migration over 24 hours in Hec1B and ARK2 cells in presence and absence of PG545 with various stimulating environments (**A, B**). Invasion of cells to a chemoattractant separated by a matrigel layer was reduced by the addition of PG545 (**C, D**). *NS: Not significant; *p<0.05, **p<0.01, ***p<0.001*.

6.3. PG545 inhibits growth in a dose-dependent manner in Type I and Type II EC.

The IC_{50} values of PG545 after 24 hours of treatment in Hec1B and ARK2 were determined by MTT assay. The IC_{50} of Hec1B cells was ~63.5 µM and 70.8 µM in ARK2 cells, (**Figures 4 A and B**). The values were calculated with GraphPad software. PG545 significantly blocked colony formation at 5 µM PG545 in both Hec1B and ARK2 cells ($p<0.05$). Maximum inhibition of colony-forming behavior was determined to be reached at 20 µM PG545 in Hec1B and 40 µM PG545 in ARK2

cells (**Figures 4 C and D**). This result was published in our report to the activity of PG545 in endometrial cancer [80]

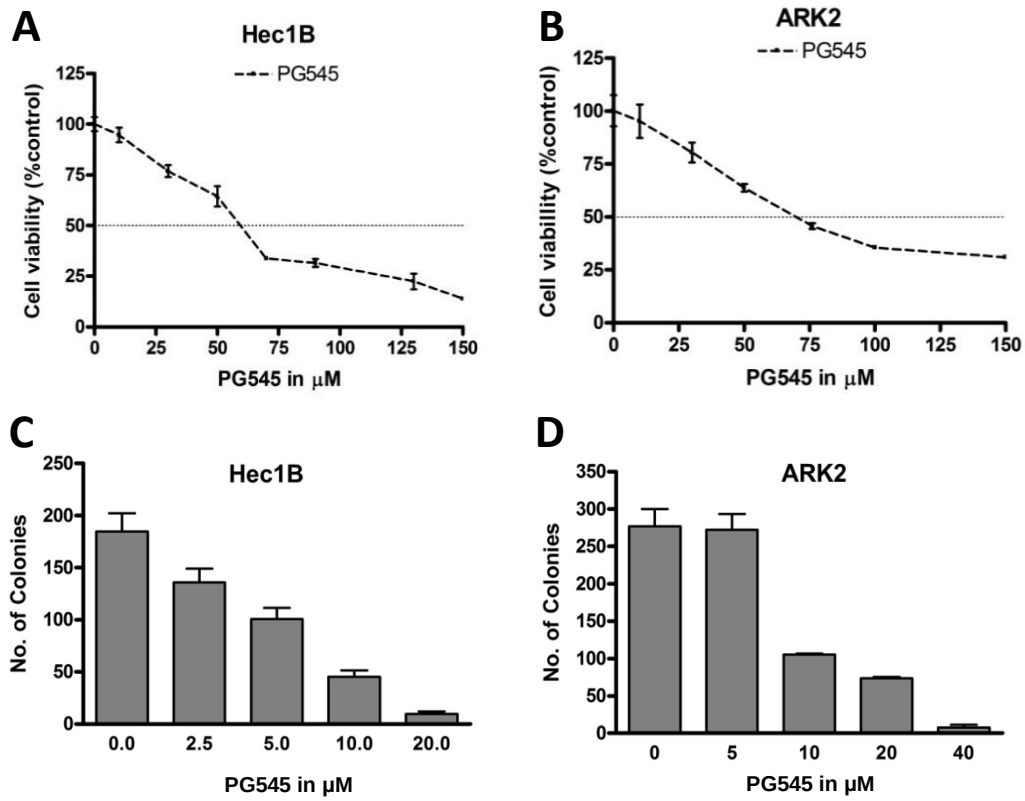

Figure 4: Cell viability of Hec1B an Ark2 cells decreases when being exposed to increasing doses of PG545. Approximated IC 50 values are highlighted by a dotted line. (**A, B**). Colony formation is equally inhibited with increasing concentrations of PG 545 **(C, D).** NS: Not significant; *p<0.05, **p<0.01, ***p<0.001.

6.4. PG545 sensitizes EC type I and II cells to standard chemotherapeutic agents.

Chemo sensitizing properties of PG5455 have been demonstrated by our group in pancreatic cancer and in ovarian cancer [70], [73]. Hence, we investigated chemo sensitizing behavior in EC type and type II cells. Added to the chemotherapeutic agents cisplatin and paclitaxel 25 µM PG 545 decreased cell viability in both Hec1B and ARK2 cells (**Figures 5 A-D**). This result indicates that synergy between the drug combinations may be present. This result was published in our report to the activity of PG545 in [80]

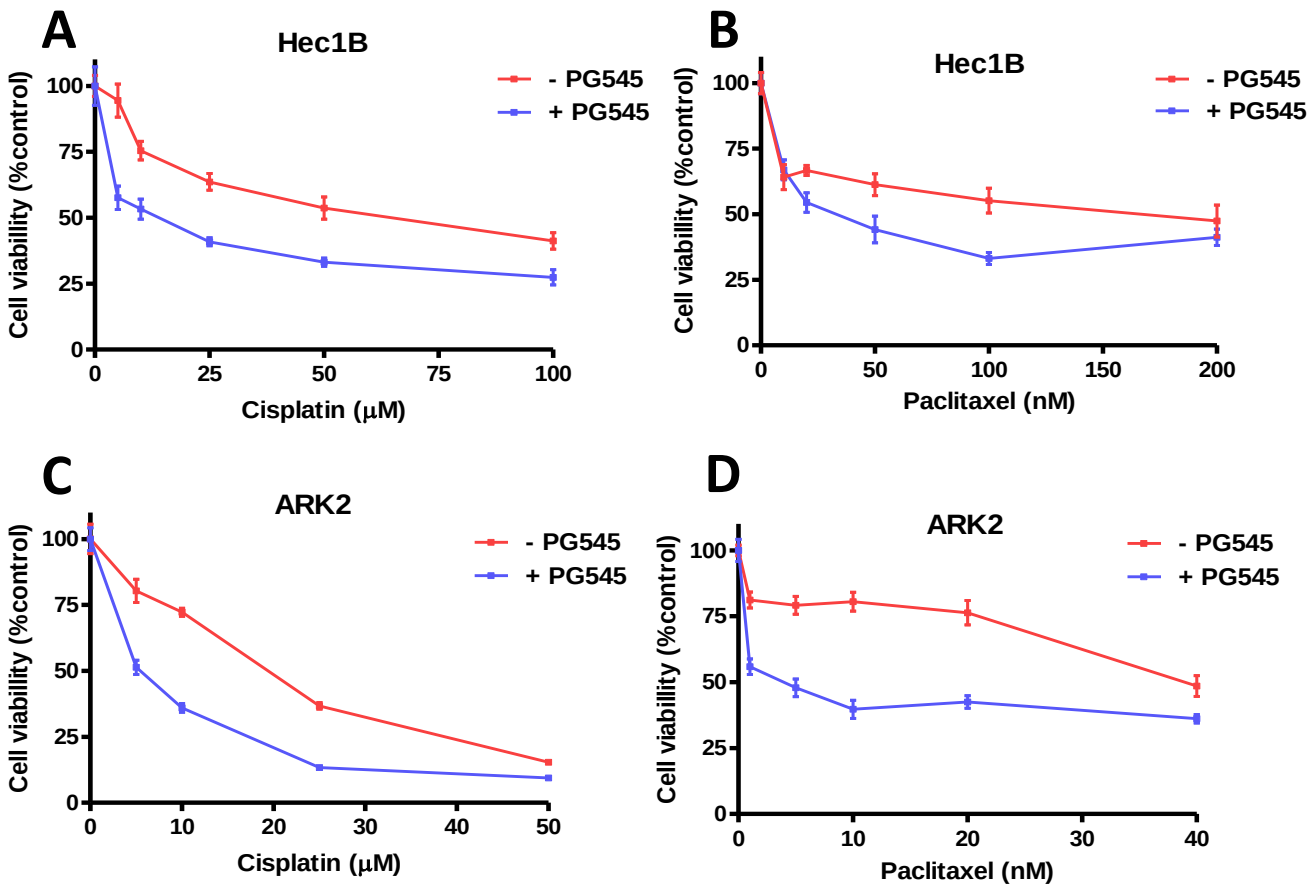

Figure 5: Hec1B and ARK2 cells were exposed to escalating doses of cisplatin and paclitaxel with (purple graph) and without (red graph) the presence of 25 µM PG545. Chemo sensitizing properties of PG545 were detected in all combinations.

6.5. PG545 exhibits strong synergistic effects with the chemotherapeutic agents cisplatin and paclitaxel *in vitro.*

Next, we assessed whether PG545 synergizes with regards to cell viability with both cisplatin and paclitaxel. We calculated the combination indices (CI) between the drugs by using constant drug ratios (multiples of the IC_{50}-values for each drug; i.e.for PG545 in ARK2 cells: 11,25 µM, 22.5 µM, 35 µM, 70 µM, 140 µM) [88]. The IC50 values for each cell and drug used to determine the presence of synergy are outlined in **table 1**.

	PG545	**Cisplatin**	**Paclitaxel**
Hec1B	60 µM	100 µM	100 nM
ARK-2	70 µM	20 µM	30 nM

Table 1. Half maximal inhibitory concentration (IC50) used for synergy experiments.

As outlined in the method section, the lower the Combination Index (CI) at a given biological effect (Fraction affected) the stronger synergistic effects are described. Very strong synergistic effects can be observed in HEC1B at lower drug concentrations and along the entire spectrum of increasing concentrations of each combination for ARK2 cells (**Figures 6 A-D**). It is important to highlight that the demonstrated values in **Figure 6** are a product of mathematical calculation and therefore are extrapolations of the experimental values. Hence the confidence intervals are increasing with more extreme biological effects. The experimental values used to determine the CI-curves range from 0.171 – 0.984 in Hec1B cells 0.22 to 0.64 in ARK2 cells. Observed and calculated synergy of PG54 were similar for both chemotherapeutics in Hec1B and ARK2 cells. This result was published in our report to the activity of PG545 in endometrial cancer [80]

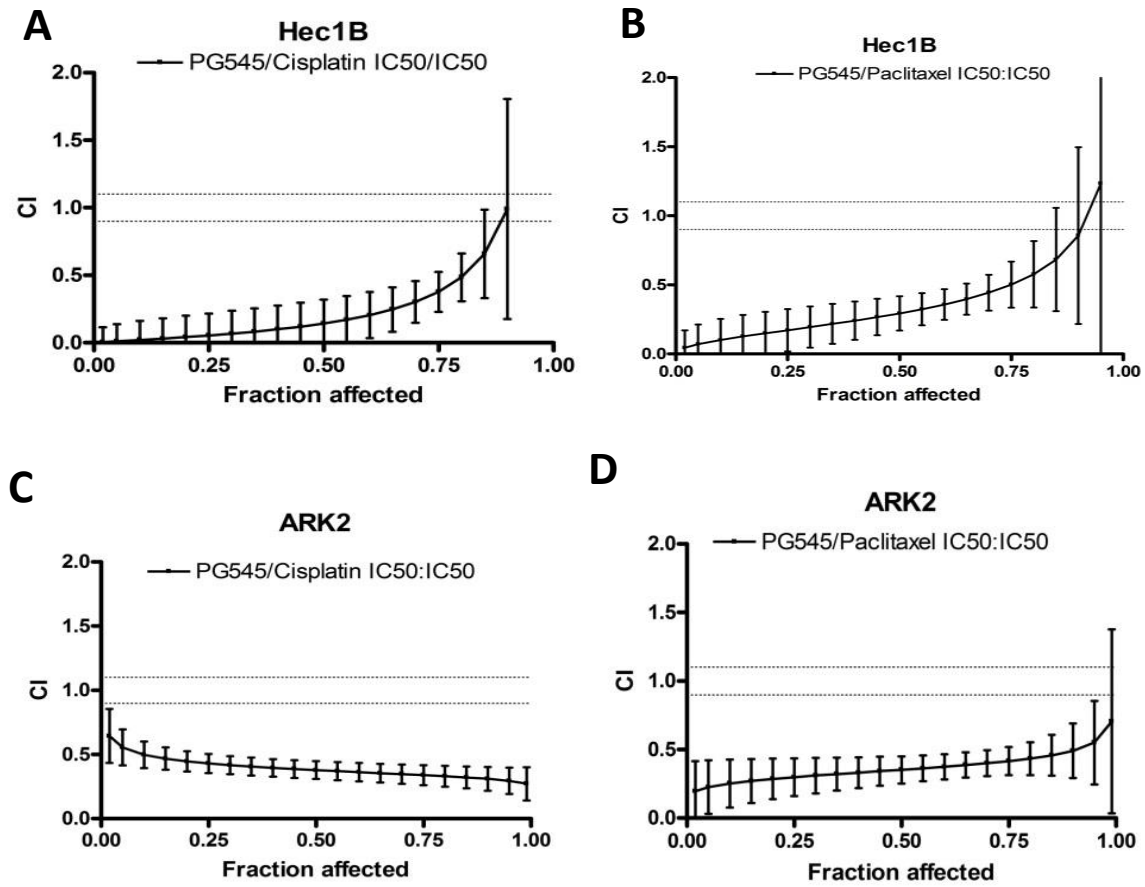

Figure 6: PG545 synergizes with the chemotherapeutic agents cisplatin and Paclitaxel *in vitro*. Hec1B and ARK2 cells were treated alone with each compound and in the combinations indicated. Constant ratios of predetermined IC50 values for each drug were used. Combination values are shown for each combination and represent mathematical calculation based on experimental values. Synergistic effects were quantified via the Chou-Talalay method. Values from 0.3–0.7 indicate strong synergy, 0.7–0.85 moderate synergy, 0.85–0.9 slight synergy, while values from 0.9–1.1 (indicated by the dotted line) describe additive and greater than 1.1 antagonistic effects.

6.6. PG545 potentiates apoptotic cell death of chemotherapy *in vitro.*

After demonstrating that PG545 synergizes with both chemotherapy drugs with regards to cell viability, we assessed whether apoptotic cell death would be increasingly observed with PG545 and its combination with cisplatin and paclitaxel. For this we used a Annexin V/ Propodium Iodine (PI) assay and treated cells for 24 hours with 20 µM PG545 alone or in combination with 20 µM cisplatin or paclitaxel (50

nM). The treatment with a single drug component showed a small, but significant difference of each compounds in both cell lines ($p<0.05$; **Figures 7 C,B,E,F**).

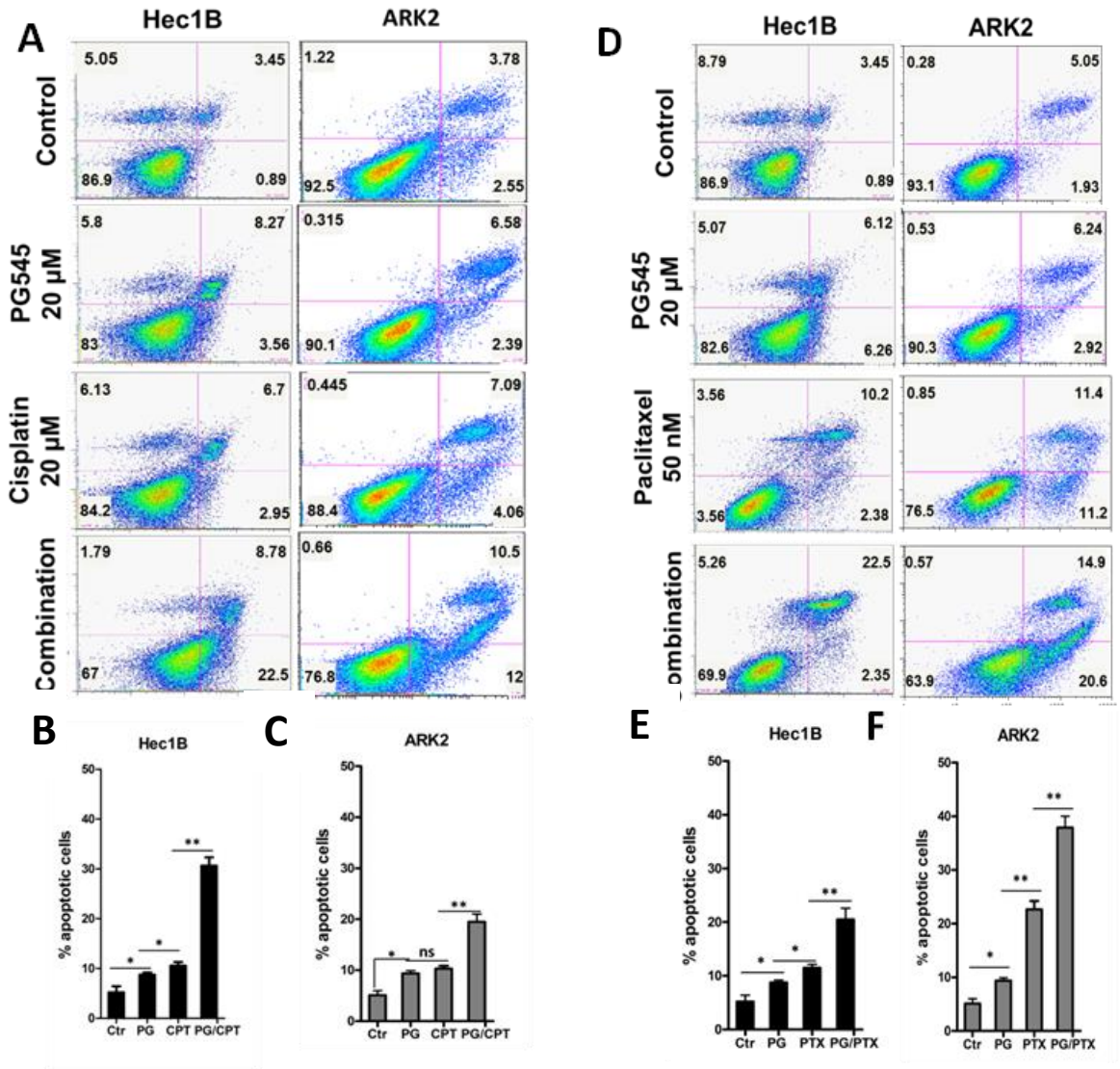

Figure 7: PG545 induces apoptosis in Hec1B and ARK2 cell alone and in combination with cisplatin and paclitaxel. Cells were stained with Annexin V/ Propodium Iodine (PI) after 24h treatment with the given drug concentration and analyzed by flow cytometry. Graphs are an illustration of the results of **Figure A** and **D** and show percentage of cells stained positive. *P-values: ns = not significant, * < 0.05, ** < 0.01.*

When PG545 was combined with either cisplatin or paclitaxel the apoptotic fraction increased substantially compared to treatments with a chemotherapeutic agent alone ($p<0.01$). Fraction of cells in early or late apoptotic cell death increased in

the platin-resistant Hec1B cells treated with cisplatin from 9.65% to 31.28% and in ARK2 cells from 11.17% to 22.5% when PG5545 was added (**Figures 7A, B, C**). Similarly, did the fraction of apoptotic cells increase in both cell lines when paclitaxel was combined with PG545 ($p<0.01$; **Figure 7 D,E,F**). This result was published in our report to the activity of PG545 in endometrial cancer [80]

6.7. PG545 alone and in combination with cisplatin and paclitaxel inhibits EC tumor growth *in vivo* and prolongs survival.

After demonstrating antitumor and chemo sensitizing effects of PG545 *in vitro,* we assess its effect *in vivo*. We established two xenograft models of type I and type II EC after injecting athymic, female nude mice subcutaneously in the right flank 10^6 Hec1B and 1.25 x 10^6 ARK2 cells. One week after inoculation and establishing that each tumor had reached a minimum size, the mice were randomized into four groups (**Figure 1**). We measured the Tumor volume every three days (in mm^3) in all four groups until the first study subject met study endpoint criteria as defined in the method section. Tumor growth was significantly inhibited by PG545 administration (20 mg/kg) compared to the PBS control (given on the same day as PG545) and chemotherapeutic regimen (given on day 7, 14 and 21 after inoculation) in both xenograft models ($p<0.001$, **Figures 8 A, B**). Furthermore, the combination of PG545 and the chemotherapy inhibited tumor growth more effectively compared to either the chemotherapeutic regimen alone ($p = 0.001$) or PG545 alone ($p = 0.05$ in Hec1B and $p= 0.01$ in ARK2 cells).

We furthermore followed the survival of the mice in the different treatment groups. In both cell lines the control had the worst survival, followed by the chemotherapy group (CPT + PTX), the PG545 group and the combination group (**Figure 8 C,D**). In the Hec1B xenografts the median survival was 33 days for mice in

the control group, 50 days for mice receiving chemotherapy and 58 days for the PG545. A median survival for the Hec1b xenografts treated with the combination regimen (PG545 + CPT + PTX) could not be determined since no substantial tumor growth was recorded in the surviving seven mice. The study was terminated on day 72. The survival depicted in the Kaplan-Meier curve was significantly improved for all treatment groups compared to the control group ($p<0.001$). No significant difference was found in the Hec1B xenograft between the chemotherapy group and the PG 545 group ($p<0.09$). Mice in the combination group survived significantly longer than both mice in the PG545 group ($p<0.001$) and chemotherapy group ($p<0.001$).

For ARK2 cells median survival for the control group was 31 days compared to 37.5 days in the chemotherapy group, 47 days in the PG545 group and 58 days in the combination group. Survival was significantly prolonged in the chemotherapy group compared to the control group ($p<0.01$) The median survival in the chemotherapy group was only 37.5 days and was comparatively less than PG545 alone with a median survival of 47 days ($p<0.05$) or the combination of both regimens with a median survival of 58 days ($p<0.001$). Still, after 63 days all ARK2 xenograft tumors met the sacrificing criteria (**Fig. 8D**). This result was published in our report to the activity of PG545 in endometrial cancer [80]

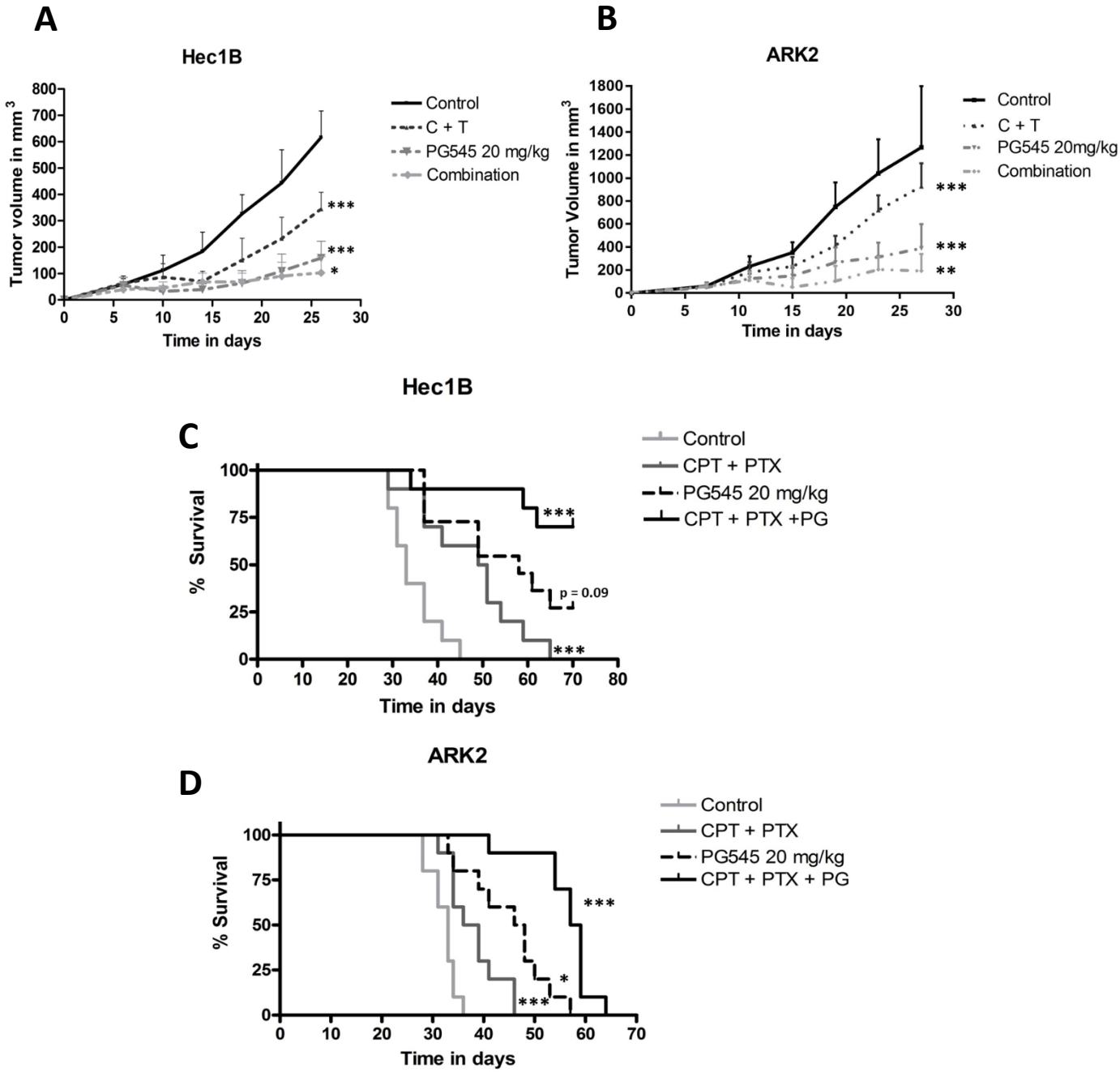

Figure 8: PG545 reduced tumor volume (**A,B**) and prolonged survival (**C,D**) alone and in combination with chemotherapy in Hec1B and ARK2 xenografts. Per Hec1B and ARK2 xenograft model ten mice were divided into four different treatment groups: Control (PBS), chemotherapy (cisplatin at 20 mg/kg and paclitaxel at16 mg/kg, PG545 (20 mg/kg) and a combination of PG545 and the chemotherapeutic agents at the same concentrations. All compounds were administered intraperitoneally. *P-values: ns = not significant, * < 0.05, ** < 0.01, ***<0.001.*

6.8. PG545 inhibits the expression of the angiogenic CD31 and proliferative Ki67 markers.

To evaluate the effect of PG545 on angiogenesis, paraffin-embedded tumor samples were assessed via immunohistochemistry for the presence of CD31, a known marker of angiogenesis. By evaluating the presence of CD31 positive cells, indicative of angio-epithelial cells, we were able to determine the intratumoral Micro Vessel Density (iMVD) [90] All PG545 treated groups displayed a reduced level of iMVD in both xenografts ($p<0.001$; **Figure 9A**). There was no significant difference observed between then control and chemotherapy groups in Hec1B ($p = 0.32$) and ARK2 ($p = 0.18$) cells. There was also no significant difference between the PG545 group or the combination group. Hence the reduction of angiogenesis is most likely due to the effects of PG545 rather than chemotherapy in the combination group. Similar results have been published previously in other solid tumor types[70], [72], [73].

We also assessed ongoing proliferation in both xenograft models at the time of death (**Figures AF and 9D, E**). Ki67 is a well-known marker for proliferation in tumors [96]. Ki67 showed was significantly higher in both the control and the chemotherapy group compared to the PG545 groups ($p<0.01$) and ARK2 ($p<0.01$) models. Notably, chemotherapy treatment did not induce a significant alteration in Ki67 expression in Hec1B tumors ($p=0.15$) relative to its control, whereas a significant change was observed in the ARK2 xenograft ($p<0.01$) potentially reflecting of the platin-resistant attributes of Hec1B cells. Parallel to CD31 expression patterns, the combined administration of PG545 and chemotherapy did not yield a significant reduction in Ki67 expression compared to PG545 alone in either xenograft model. This lack of significance is likely attributable to the time between the last chemotherapy

administration, leading to different treatment du rations between the two groups. This result was previously published by our group [80]

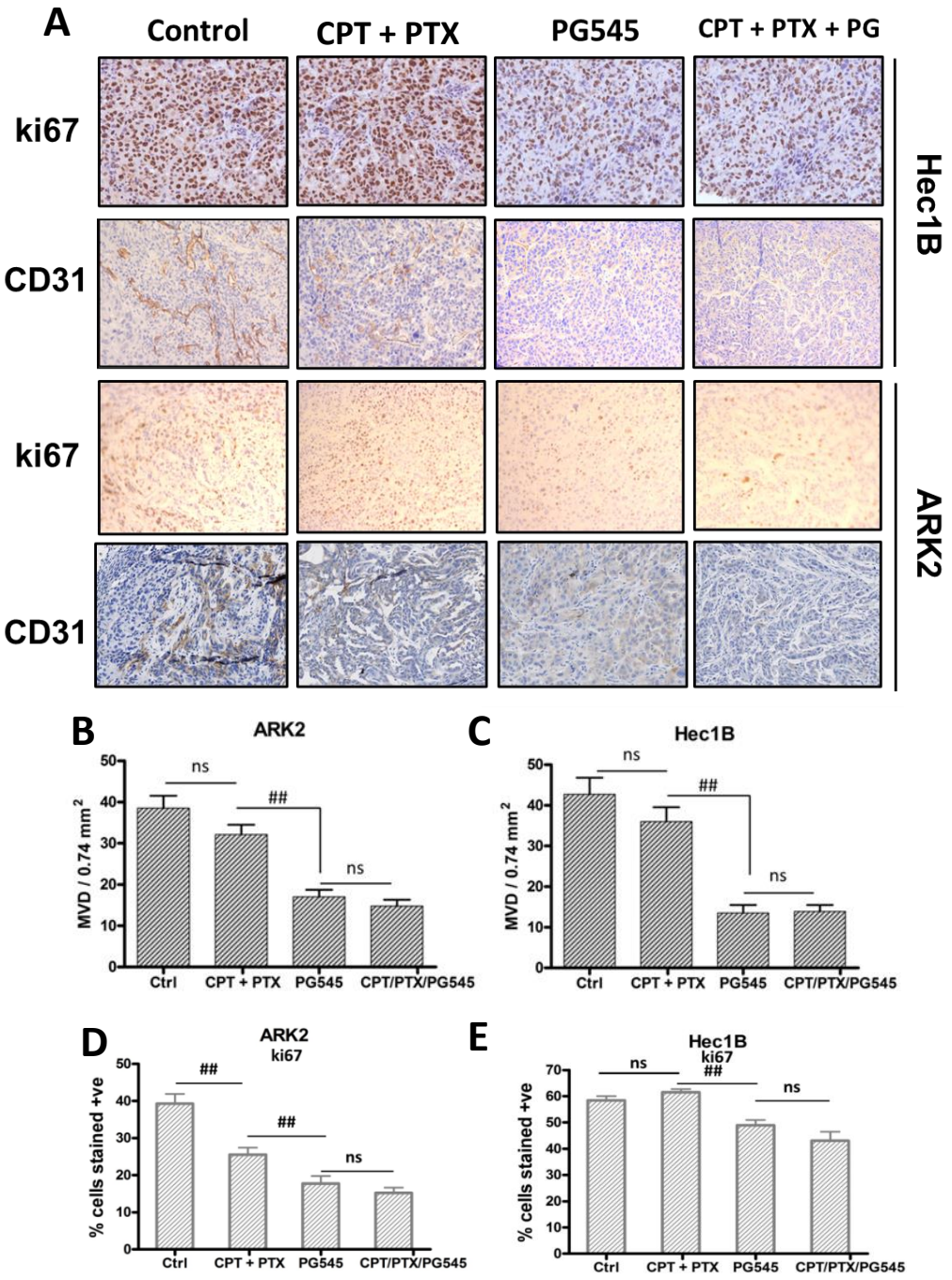

Figure 9: PG545 demonstrates antiangiogenic and antiproliferative effects in vivo based on immunohistochemistry. Tumor samples of both Hec1B and ARK2 xenografts were analyzed after immunostaining with ki67 and CD31 (A). Intratumoral Micro Vessel Density (iMVD) was assessed in 20X magnification based on 3 fields per analyte (B,C). The ratio of ki67 psotive cells was determined based on 5 fields per analyte via ImageJ software and the ImmunoRatio Add-on (D,E). *P-values: ns = not significant, #< 0.05, ##< 0.01.*

6.9. PG545 induces autophagy in EC.

We sought to further explore potential mechanisms for the synergy observed between PG545 and chemotherapy. Since autophagy is a known mediator of chemoresistance, we decided to investigate the effects of PG545 on autophagic flux in EC cells. When exposed to increasing concentrations of PG545 both Hec1B and ARK2 cells demonstrated an increase of LC3BII, a protein present in the membranes of autophagosomes and hence a marker for autophagic processes in the cell (**Figures 10 A, B**). To better quantify the upregulation of LC3BI to LC3BII densitometric measurements below the blots were provided. In concordance with the elevation in LC3BII levels, immunofluorescence (IFC) analysis of autophagy utilizing cyto-ID staining demonstrated that PG545 induced autophagy in Hec1b and ARK2 cells (**Figure 10 C**) [97]. Quantification of the autophagosome fluorescence displayed in **Figure 10 E** illustrates via the Corrected Total Cell Fluorescence (CTCF) an increase of autophagy in both cell lines ($p<0.001$).

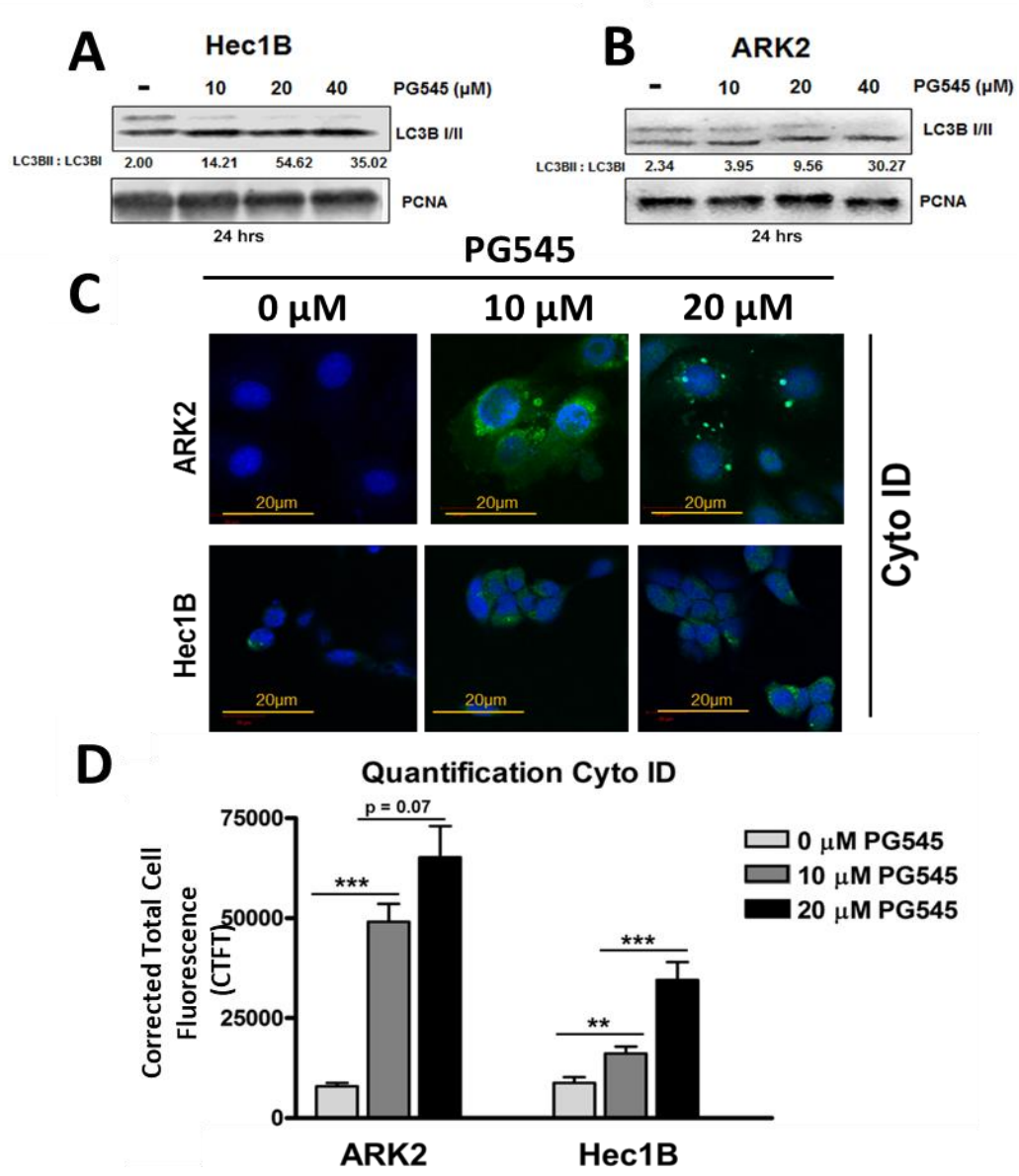

Figure 10: PG545 induces autophagy in EC type I and type II cells. Autophagic fin Hec1B (**A**) and ARK2 (**B**) cells. Cells were either treated with 10 μM and 20 μM PG545 for 24 hours. Cell lysates were analyzed by Western blot using antibodies to LC3BI/II. Densitometric quantification of the LC3B I:II ratio was measured via image J software. Immunoblot analyses are shown for Hec1B and ARK2 cell lysates treated with 10,20 and 40 μM PG545 for 24 hours (**B,D**)**.** Cyto ID staining shows autophagosome formation in ARK2 and Hec1B cells when treated with PG545 (**E,F**). Quantification of Corrected Total Cell Fluorescence (CTCF) was calculated p-*values: ns = not significant, * < 0.05, ** < 0.01, ***<0.001.*

Although LC3BII was initially described as a marker for autophagy, it has also been shown that upregulation in LC3BII could be due to inhibition of the last step of autophagy, the fusing of the autophagosome with a lysosome [98], [99]. Hence, we investigated the levels of p62 (SQSTM1) another marker of autophagy. We incubated Hec1B, ARK2, RL95 and Ishikawa cells for 24 hours with 20 μM of PG545 with and without 20 μM of the established autophagy inhibitor chloroquine (CQ) to determine whether the autophagic processes induced by PG545 would be reversible. The administration of PG545 to Hec1B and ARK2 cells led to reduced levels of p62 and an increase in the levels of LC3BII (**Figures 11A, B**). Addition of CQ to PG545 reversed the expression of both these proteins, providing clear evidence of PG545 induced autophagic flux. Similarly, RL95 and Ishikawa cells exhibited an autophagic response to PG545 treatment, mirroring the observations in Hec1B and ARK2 cells (**Figures 11C, D**). However, it is worth noting that in the Ishikawa cell line, CQ failed to rescue p62 levels, suggesting a differential response to autophagy modulation in distinct cellular contexts (**Figure 11D**).

Another reliable monitoring method involves the use of a fluorescent-tagged Cherry-GFP-LC3B construct following autophagy induction [100]. By measuring the fluorescence of the pH-sensitive GFP, which is degraded by the acidic content of autolysosomes and the stable mCherry protein, autophagic flux in a cell can be visualized at different stages. Early autophagic processes with the presence of the less acidic autophagosomes exhibit more green fluorescence with this construct, while later stages of autophagy characterized by an increase autolysosome, are reflected in a less green fluorescence in

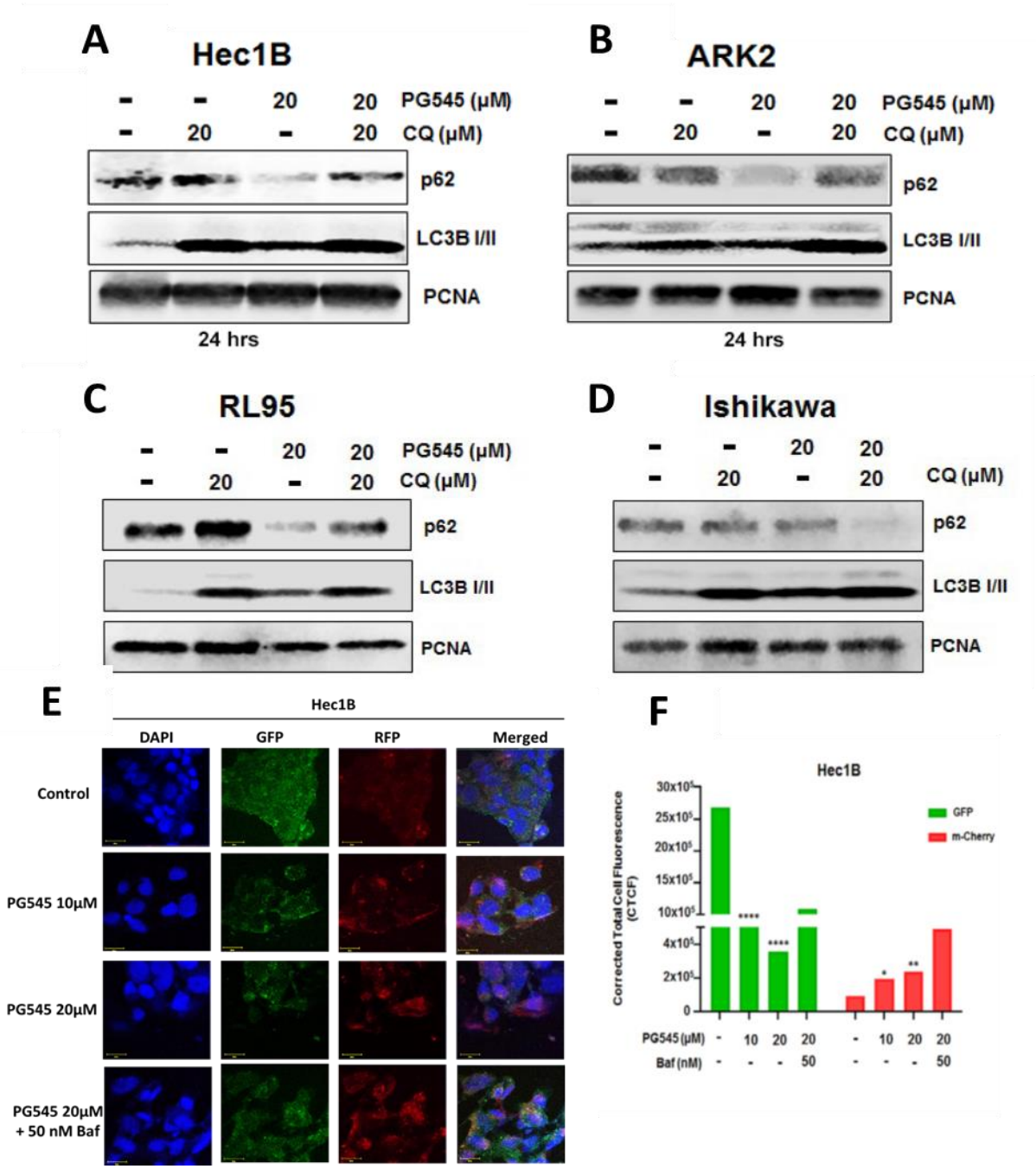

Figure 11: Further evidence that PG 545 elicits autophagic flux in different EC cells. The presence of p62 and LC3B were analyzed via western blot in Hec1B, ARK2, RL95 and Ishikawa cells treated for 24 hours with 20 μM PG545 and/or with 20 μM chloroquine (**A,B,C,D**). After transfection with a mCherry-GFP-LC3B plasmid, autophagic flux was assessed in Hec1B cells treated with 10 μM and 20 μM PG545 for 24 hours and co-treated with 50 nM Bafilomycin for 12 hours. Confocal microscopy showed changes in autolysosome formation. Quantification of Corrected Total Cell Fluorescence (CTCF) was determined by using ImageJ software (**E,F**). *P values: ns = not significant, * < 0.05, ** < 0.01, ***<0.001, ****<0.0001.*

and comparatively more red fluorescence. Following transient transfection of Hec1B cells with Cherry-GFP-LC3B for 48 hours, treatment with 10 and 20μM PG545 resulted in increased mCherry-positive signals in treated cells compared to untreated controls, indicating activated autophagic flux ($p<0.0001$). Co-treatment with Bafilomycin A, preventing autophagosome-lysosome fusion, exhibited more GFP staining in the merged panel, suggesting reduced autolysosomal activity. This result was published in our report to the activity of PG545 in endometrial cancer [80]

6.10. PG545 elicits ER stress and unfolded protein response.

We have shown that PG545 induces autophagy. Interestingly, PG545 has been shown to inhibit autophagy in cervical and glioblastoma cell lines by inhibiting heparanase-induced autophagic activation a mechanism of chemoresistance and tumor proliferation in these cells [75]. To further investigate the differences between the result of this study and the prior study we investigated possible mechanism by which PG545 may induce autophagy rather than inhibit it in EC cell lines. Based on prior literature endoplasmatic reticulum stress is a well described inducer of autophagy [101]. Autophagy is triggered as survival mechanism by ER stress trying to salvage unfolded protein response (UPR), which ultimately leads to cessation of function and cell death [102]. As previously established PG545 alters growth factor signaling, which is a known potent trigger of ER stress. Hence, we sought to examine whether PG545 would induce ER stress and therefore activate autophagy as adaptive response signaling [103], [104]. For this we first treated Hec1B and ARK2 cells with 20 μM PG545 for 15, 30 and 60 min and then stained the cells with Blue-White-DPX dye, a photostable probe selective to ER in live cells. Increased absorption of the dye reflects increased ER activity and indicates ER stress in the cells. We observed a significant increase in dye uptake in both Hec1B and ARK2 cells demonstrating that PG545

triggers ER stress in these cells compared to the control (**Figure 12A-C**). Fluorescence was quantified as CTCF.

Since PG545 treatment results in increased ER activity indicating ER stress in both Hec1B and ARK2 cell lines, we conducted an analysis on several molecular markers associated with ER stress to confirm that PG545 indeed acts as a trigger. On western blot analysis PG545 alters well-established ER stress pathways within a time frame of 6 to 24 hours (**Figure 12D**). One prominent mechanism involves the phosphorylation of the eukaryotic initiation factor 2 (eIF2) α subunit by protein kinase R-like endoplasmic reticulum kinase (PERK) [105], [106]. This process is recognized for downregulating protein synthesis in response to cellular stress conditions. Once activated it triggers the expression of stress-induced transcription factors C/EBP homologous protein (CHOP) or growth arrest and DNA damage 153 (GADD153) [107]. In PG545-treated EC cells, the activation of PERK, evidenced by phosphorylation at Thr980, coupled with an increase in CHOP/GADD153 levels, signifies the inhibition of protein synthesis and the initiation of apoptosis in response to ER stress. PG545 treatment resulted in a substantial increase of the ER chaperone, GRP78/BiP, indicating that unfolded ER proteins, a sign of ER stress, are increasingly accumulated under PG545 treatment [108]. Notable differences between the cell lines are that the activation of PERK and inositol-requiring enzyme 1 (IRE) was considerably more pronounced in ARK2 cells compared to Hec1B cells (**Figure 12E**).

Additionally, the calcium-dependent chaperone, Calnexin, well-documented for its involvement in apoptosis, exhibited an upregulation after 24 hours of PG545 treatment in both cell lines, providing further evidence of prolonged ER stress [109].

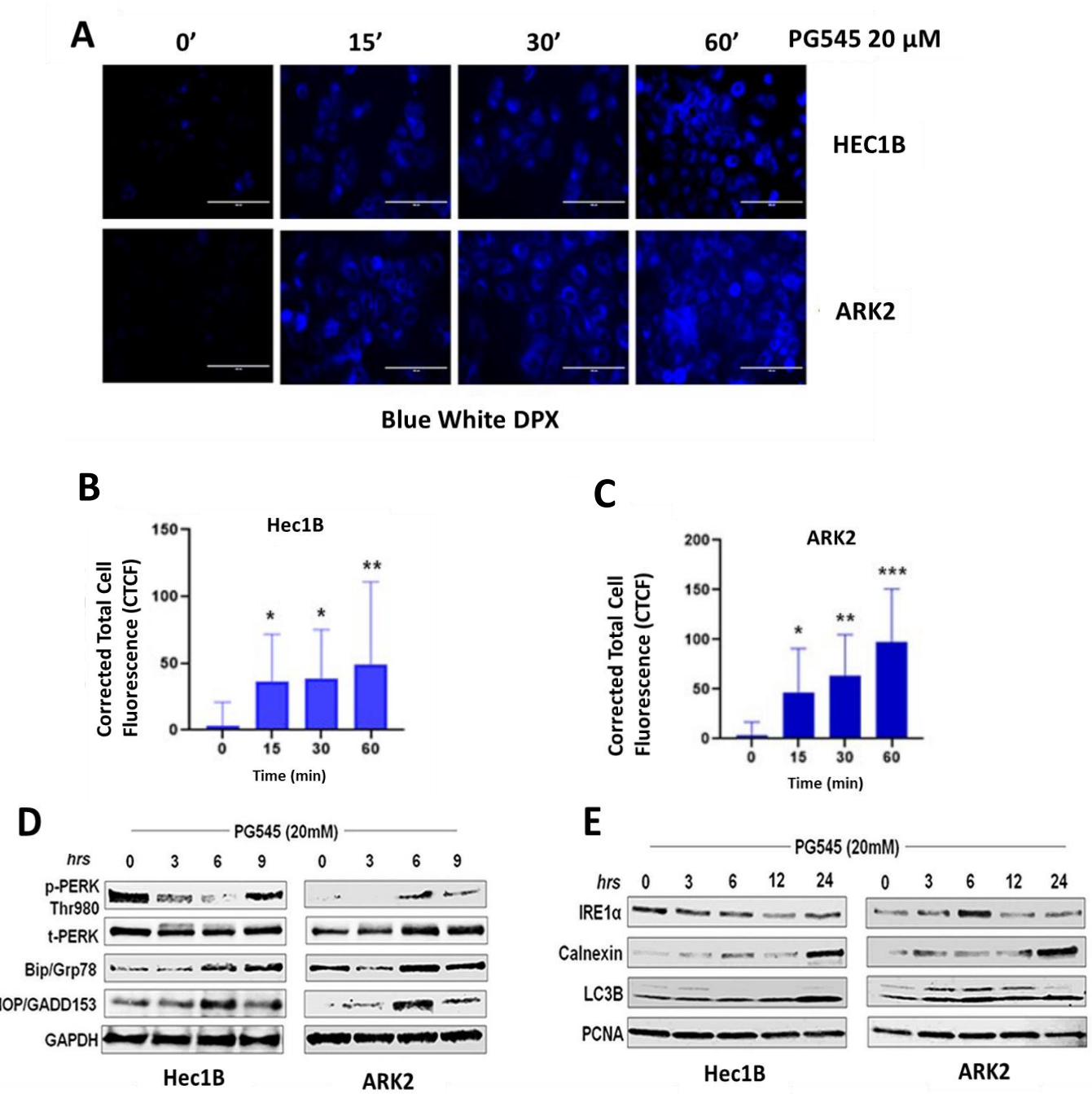

Figure 12: Treatment with 20 µM of PG545 for 15 – 60 min PG545 induces ER stress in Hec1B and ARK 2 cells. ER activity is assessed using blue-white DPX dye **(A)**. The CTCF was quantified via ImageJ software (**B,C).** *P values: * < 0.05, ** < 0.01.* Samples of Hec1B and ARK2 cells were analyzed after treatment with 20 µM PG545 for the presence of ER stress markers. This work was conducted by Dr. Bhattarchayan

This also connects PG545 treatment mechanistically to apoptotic cell death observed in earlier experiments. Lastly, we also see concomitant upregulation of LC3BII seen in earlier experiments linking PG545 to autophagy via induction of ER stress. This result was published in our report to the activity of PG545 in endometrial cancer [80]

6.11. ER stress caused by PG545 induces autophagy as homeostatic response.

The ER holds an important role in protein synthesis and maintaining cellular homeostasis. When ER stress accumulates proteins that are misfolded or remain unfolded in the Unfolded Protein Response [101]. Several salvaging pathways are activated including autophagy as we have established. In PG545 treatment we have seen that marker of ER stress increase. We have seen that an indicator of autophagy LC3BII increases as well. Hence, we sought to determine whether the autophagic flux observed is caused by PG545 induced ER stress and whether it would be reversible when ER homeostasis is reinstated despite PG545 treatment. For this we supplemented Hec1B and ARK2 cells, treated with or without 20 µM of PG545, with an additional 1 µM of melatonin for 30 min, a known promoter of ER homeostasis and suppressor of ER stress [110]. We subsequently used the previously used staining techniques of the ER tracker Blue-White-DPX (blue) and the autophagy tracker cyto ID (green). While we see an upregulation of ER activity and autophagic flux in Hec1B (**Figure 13 A,C**) and ARK2 (**Figure 13 B,D**) cells under PG545 treatment alone, melatonin reverses this effect. Integral fluorescence of five representative fields marking ER activity decreases significantly for Hec1B ($p<0.01$) and ARK2 ($p<0.01$) cell lines. Autophagic flux simultaneously decreases significantly for both cell lines ($p <0.01$ in Hec1B and $p<0.05$ in ARK2 cells) providing further proof next to LC3BII upregulation that autophagy is induced by ER stress under PG545 treatment. Parallel

western blots assessing the presence of ER stress markers show a similar pattern. PG545-mediated upregulation of CHOP, BiP/Grp78 and LC3B are reversed when cells are treated with melatonin (**Figure 12 E**). This result was published in our report to the activity of PG545 in endometrial cancer [80]

6.12. PG545 in combination with cisplatin escalates ER stress in EC cells.

At this point we have demonstrated that PG545 shows strong synergy with both chemotherapeutic compounds, cisplatin and paclitaxel. Furthermore, we showed that autophagy is likely a cell preserving mechanism to salvage misfolded proteins induced by ER stress. To further link drug synergy with the proposed mechanism, we combined PG545 and cisplatin to investigate the effects on ER stress and autophagic markers (**Figure 13 F**). When we combined 5 μM of cisplatin with 20 μM of PG 545 we encountered increased expression of the well- established ER stress markers BiP/Grp78 and CHOP with simultaneous upregulation of LC3BII. This shows that synergy between both drugs is likely mediated through ER stress.

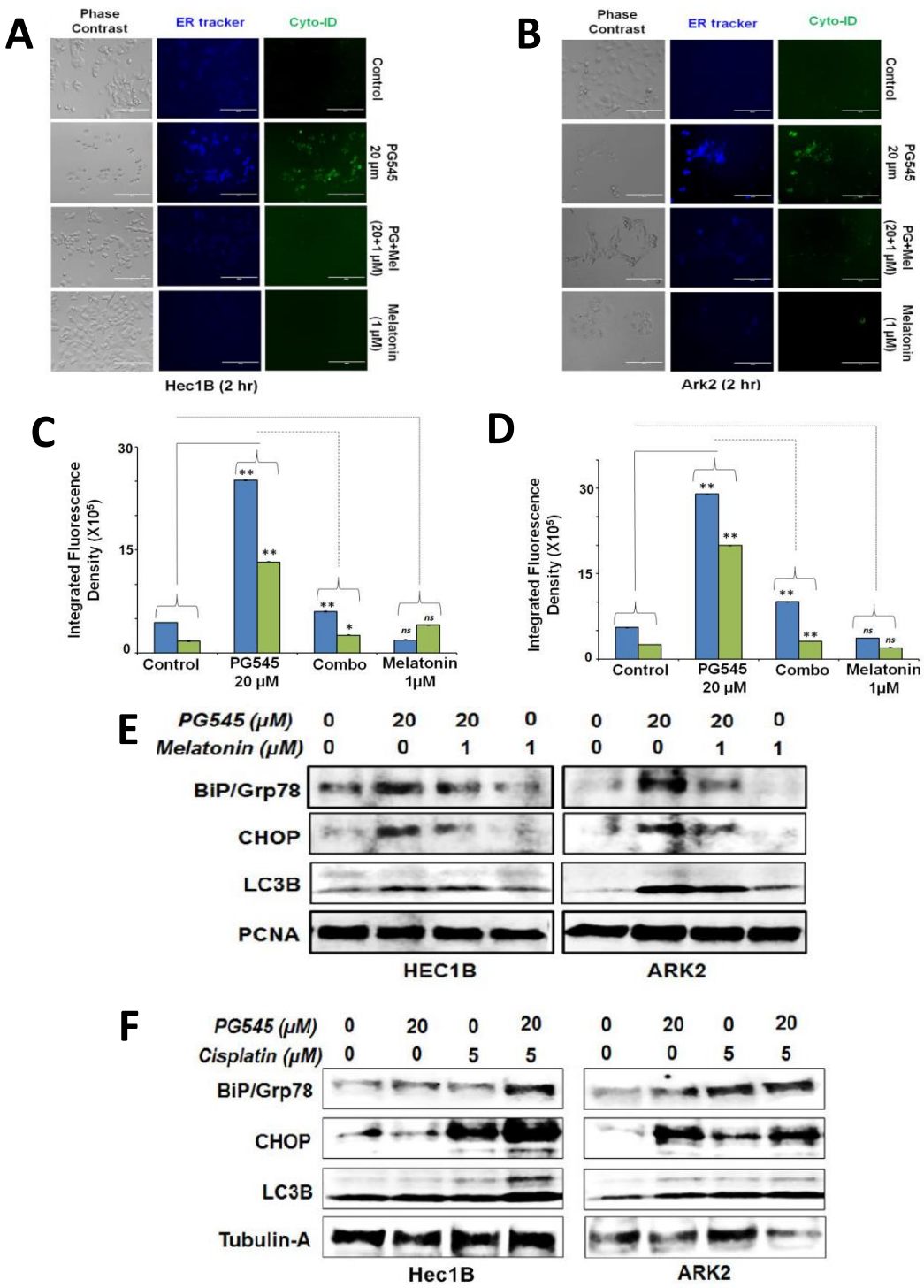

Figure 13: PG545 induced autophagy by ER stress. ER activity marked by Blue-White DPX stain decrease simultaneously with autophagy (cyto ID) signals when treated with 1 µM melatonin for 30 min **(A, B)**. Integrated fluorescence density was measured via ImageJ software **(B and D)**. *P values: ns = not significant, * < 0.05, ** < 0.01.* Immunoblots of Hec1B and ARK2 cells exposed to PG545 for 12 hours and/or melatonin demonstrate reduced expression of BiP/Grp78, CHOP and LC3BII **(E)**. Addition of cisplatin (5 µM) to PG545 escalates expression of ER stress markers BiP/Grp78 and CHOP (**F**).

6.13. The effect of PG545 can be potentiated when chloroquine, a known autophagy inhibitor is added.

Autophagy can act as a double-edged sword, in most cases a mechanism promoting cell homeostasis and survival, in some case inducing autophagic cell death [111]. In PG545 we demonstrated that it is triggered by ER stress as a mechanism of homeostasis and to promote cell survival. Hence, we hypothesized that if autophagy were inhibited the antitumor effects of PG545 could be increased. For this we combined the known autophagy inhibitor chloroquine, for which we demonstrated that it blocks autophagic flux in the cell when added to PG545 (**Figure 8**). We added 20 µM chloroquine to increasing concentrations of PG545 in Hec1B, ARK2, Ishikawa and RL95 cells for 48 hours and analyzed cell viability in MMT assays. (**Figure 14 A-D**). Co-treatment with CQ significantly enhanced the cytotoxicity of PG545 as seen in the change in the IC50 values to a significantly lower levels in all four cell lines ($p<0.001$). and lowered up to 3.5-fold in the Ishikawa cell line from 112 µM to 33 µM. The least shift in IC50 could be observed in the Hec1B cell lines whose IC50 was reduced from 66 µM to 36 µM. Only at 100 µM PG545 in Hec1B we did not see a significant difference likely due to the high biological impact of PG545 alone at this concentration.

To determine if combination of PG545 + CQ resulted in cell death, we incubated the four EC cell lines for 24 hours with 20 µM of PG545 and/or 20 µM chloroquine and analyzed cell lysates for PARP cleavage an established marker for late apoptosis. All four cell lines demonstrate a marked increase of cleaved PARP compared to the control or each drug alone (**Figure 14 E**). This demonstrates that the addition of the autophagy inhibitor chloroquine increases the antiproliferative properties of PG545 *in vitro*.

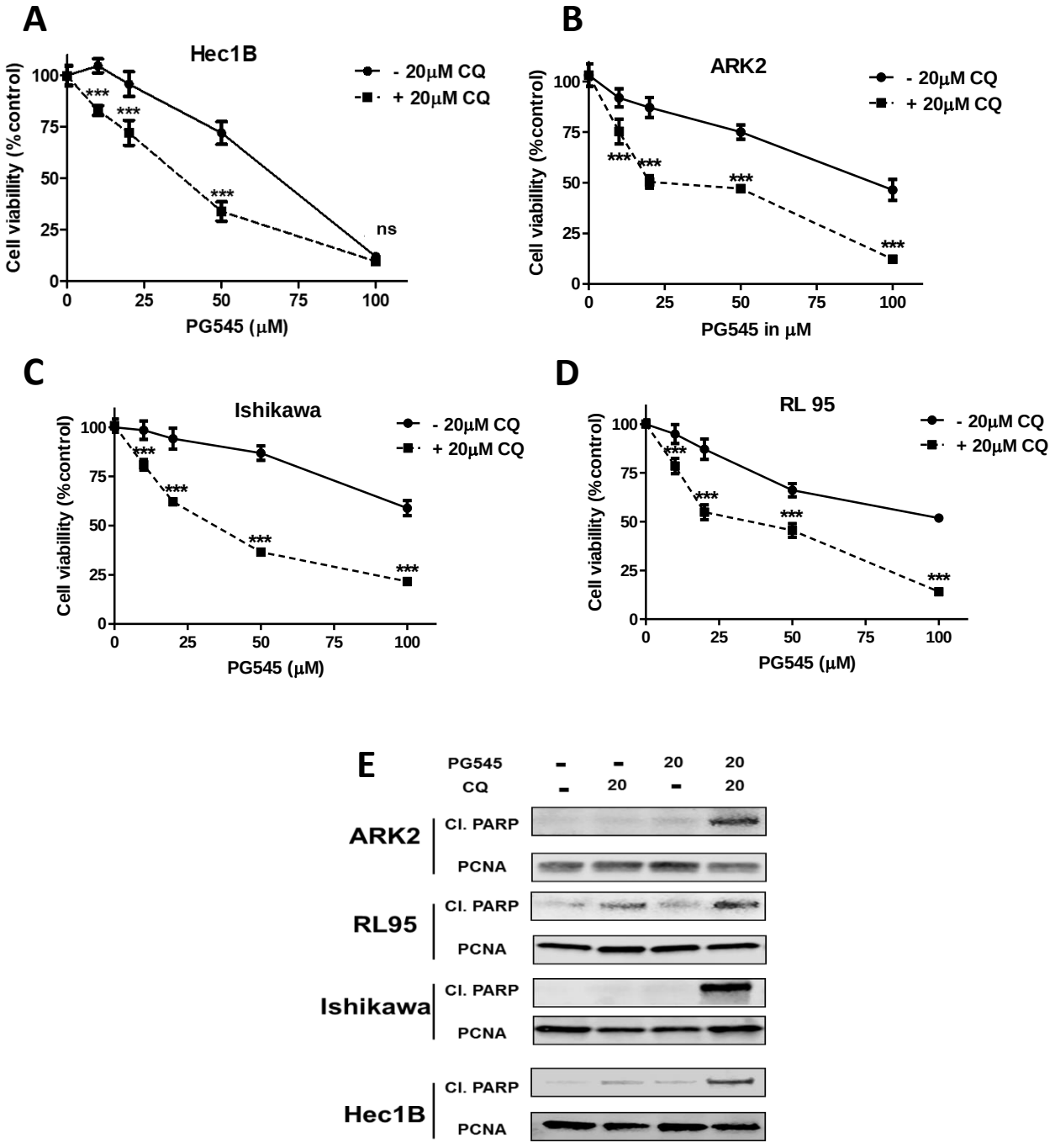

Figure 14. Addition of chloroquine potentiates antitumor effects of PG545. Cell viability of ARK2, RL95, Ishikawa and Hec1B cells measured by MTT assay with increasing concentrations of PG545 with and without Chloroquine (20 μM, **A-D**). E. Immunoblot analysis of cell lysates harvested from ARK2, RL95, Ishikawa and Hec1B cells treated with PG545 (20 μM) alone and/or treated with Chloroquine (20 μM) for 24 hours with anti-cleaved PARP and anti-PCNA antibodies (**E**). *P values: ns = not significant, * < 0.05, ** < 0.01.*

6.14. PG545 synergizes with chloroquine in EC cell lines.

Parallel to our experiments regarding synergistic effects between PG545 and the chemotherapeutic regimen cisplatin and paclitaxel, we then investigated the interaction of both drugs on cell proliferation measured via MTT assay. For this we used the IC_{50} listed **table 2** determined by MTT assays.

	Chloroquine	**PG545**
Ishikawa	160 µM	100 µM
Hec-1B	80 µM	60 µM
RL95	100 µM	100 µM
ARK-2	160 µM	70 µM

Table 2. Half maximal inhibitory concentration (IC50) used for synergy experiments

When combining multiples of IC_{50}-ratios we found that PG545 and Chloroquine are synergizing in all four cell lines (**Figure 15**). Effects were least pronounced in Hec1B cells with CI-values ranging from 0.5 to 1.6. Notably, in ARK2, Ishikawa and RL95 strong synergism was observed between PG545 and chloroquine. The CI values at 50% fraction affected are 0.574 for Hec1B; 0.264 for ARK2 *RL95:* 0.147 for RL95 and 0.181 for Ishikawa cells.

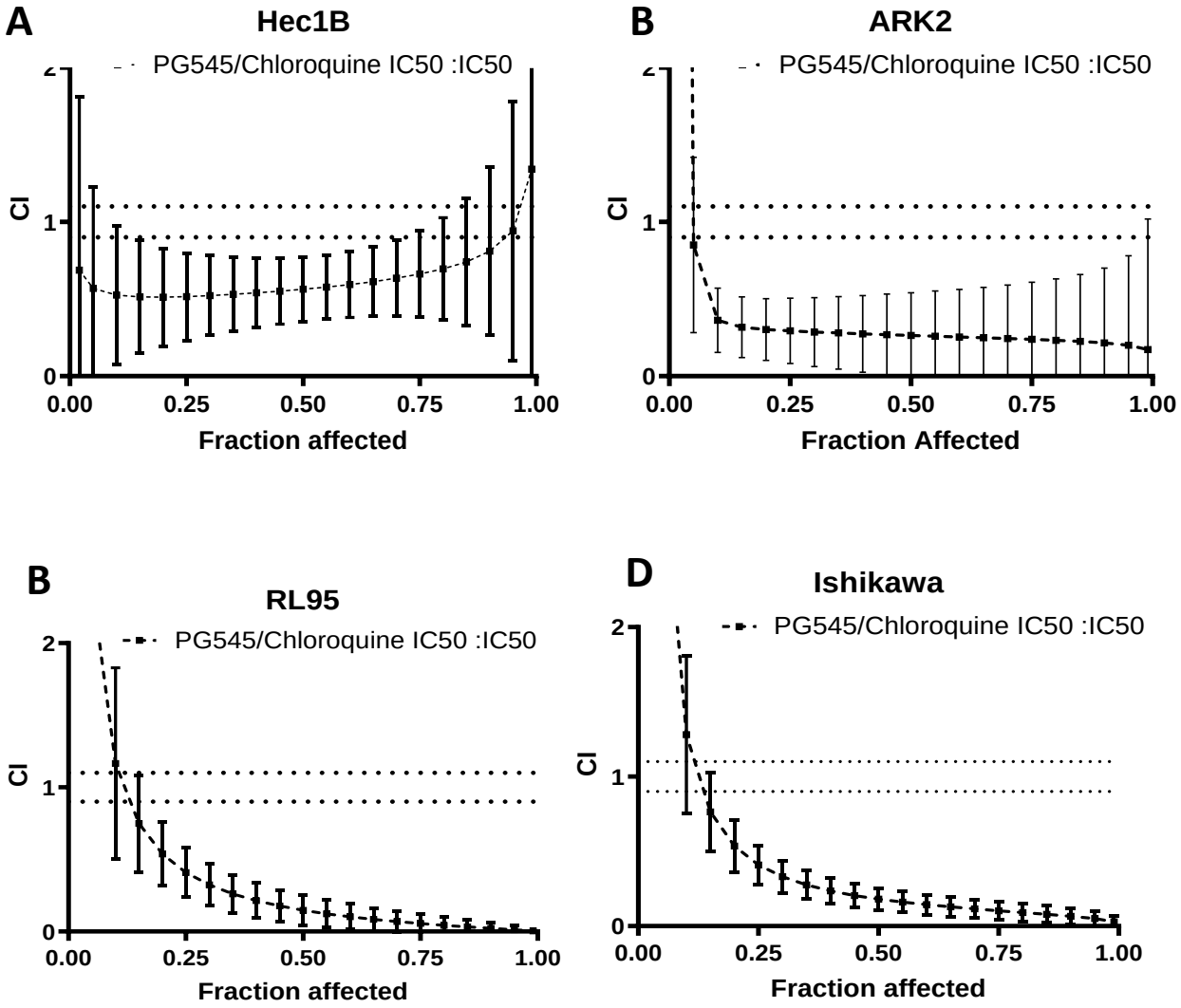

Figure 15: PG545 and chloroquine synergize in EC cells. Combination indices (CI) were determined via the Chou-Talalay Method between PG545 and choloroquine an autophagy inhibitor. CI between 0.3–0.9 shows synergism, 0.9–1.1 additive effect, and 1.1 – 2 antagonism

6.15. Synergy between PG545 and Cisplatin or paclitaxel is preserved under Autophagy inhibition.

As we established PG545 triggers autophagy in endometrial cancer cells. In this context, autophagy serves as a compensatory mechanism to preserve cellular homeostasis, given that PG545 induces significant endoplasmic reticulum (ER)

stress in the cells. We experimentally confirmed that the combination of PG545 and cisplatin escalates ER stress in Hec1B and ARK2 cells. Our findings further indicate that inhibiting autophagy with chloroquine enhances the effects of PG545 alone in endometrial cancer cells. In our final experiment, we aimed to investigate whether blocking autophagy would impact the synergistic drug combination of PG545 with the chemotherapeutic drug cisplatin and paclitaxel. Our hypothesis was that blocking autophagy could further potentiate the synergistic effects of cisplatin with PG545. The concept of combining multiple drugs targeting pathways interacting with each other refers to synthetic lethality [112].

In order to assess whether the combination between CQ and PG545 could potentiate chemotherapy induced cytotoxicity over PG545 induced sensitization of chemotherapy induced cytotoxicity, we determined synergism in a three-drug-combination with PG545/CQ treated as a single drug with paclitaxel and/or cisplatin alone as drug #2. To be able to calculate CI values between three drugs, it is necessary to reformulate the equation by considering (cisplatin and /or paclitaxel as drug A and consider the combination of drug B (PG545) + drug C (CQ) as drug D as one drug[113]. Therefore, the equation will consider the combination indices for drugs A+D. This maneuver enables the CalcuSyn software to calculate CI values involving all three components.

Initially we assessed areas of great synergy between PG545 and CQ in order to confirm that varying concentrations would synergize with each other (**Figure 15 A**). We used ARK2 cells for assessment. Therefore, we plotted multiples of the IC50 concentrations of PG545 and CQ against each other to assess the experimental CI values of each combination with the Chou-Talalay method. Starting with IC50 for PG545 at 70µM and for Chloroquine at 80µM respectively to have CI values in the

synergistic range. CI values at 0.3–0.9 represent synergism (Green), at 0.9–1.1 represent the additive effect (Yellow), and at 1.1 – 1.7 values indicate antagonism (Red). Interestingly, synergistic effects could only be observed when the concentration of PG545 was 8.75 µM or higher and reflects autophagic responses to PG545 treatment in our previous experiments when autophagy was observed only at concentration of 10 µM and higher.

Based on our detailed and extensive analyses as described above, we defined a new fixed ratio of PG545 and CQ of 35 µM and 20 µM respectively, which solely showed CI values below ranging from 0.012 to 0.749, as compound D (**Figure 16**). This new compound D was assessed for its synergy with cisplatin and paclitaxel via the Chou-Talalay-Method (**Figures 17 A and C**). All experimental values for cisplatin and paclitaxel containing combinations were below 1. The calculated CI value curve for cisplatin and compound D was below 0.9 from 0.05 (0.346) Fraction affected to 0.90 (0.876). The calculated CI values for Paclitaxel and compound D ranged from Fraction affected 0.3 (0.819) to 0.9 (0.623) below one. Synergy remains between compound D and the chemotherapeutic agents just as in PG545 and chemotherapy (**Figure 6**). To further illustrate what this means with a “compound” which is more effective than PG545 alone, we plotted the MTT data values indicating cell viability with each concentration used (**Figures 17 B and D**). With addition of CQ to the combination of PG545 and cisplatin or paclitaxel, IC50 values could be significantly reduced. Therefore, based on this data, we conclude that autophagic inhibition by CQ does not negatively influence the synergism between PG545 and chemotherapy, but rather potentiates its effects.

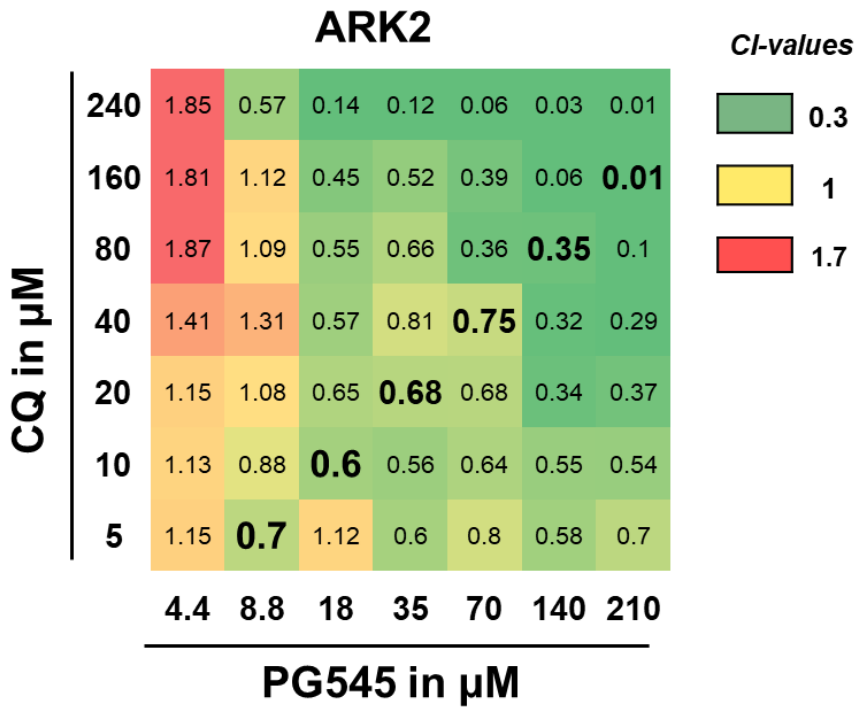

Figure 16: Experimental combination indices (CI) values were determined via the Chou-Talalay Method between PG545 and chloroquine in ARK2 cells across 49 different experimental concentrations. CI between 0.3–0.9 shows synergism (Green), 0.9–1.1 additive effect (Yellow), and 1.1 – 1.7 antagonism (Red). The drug ratio of PG545 (70 µM) and chloroquine (40 µM) used for experiments in *Figure 16* are bolded.

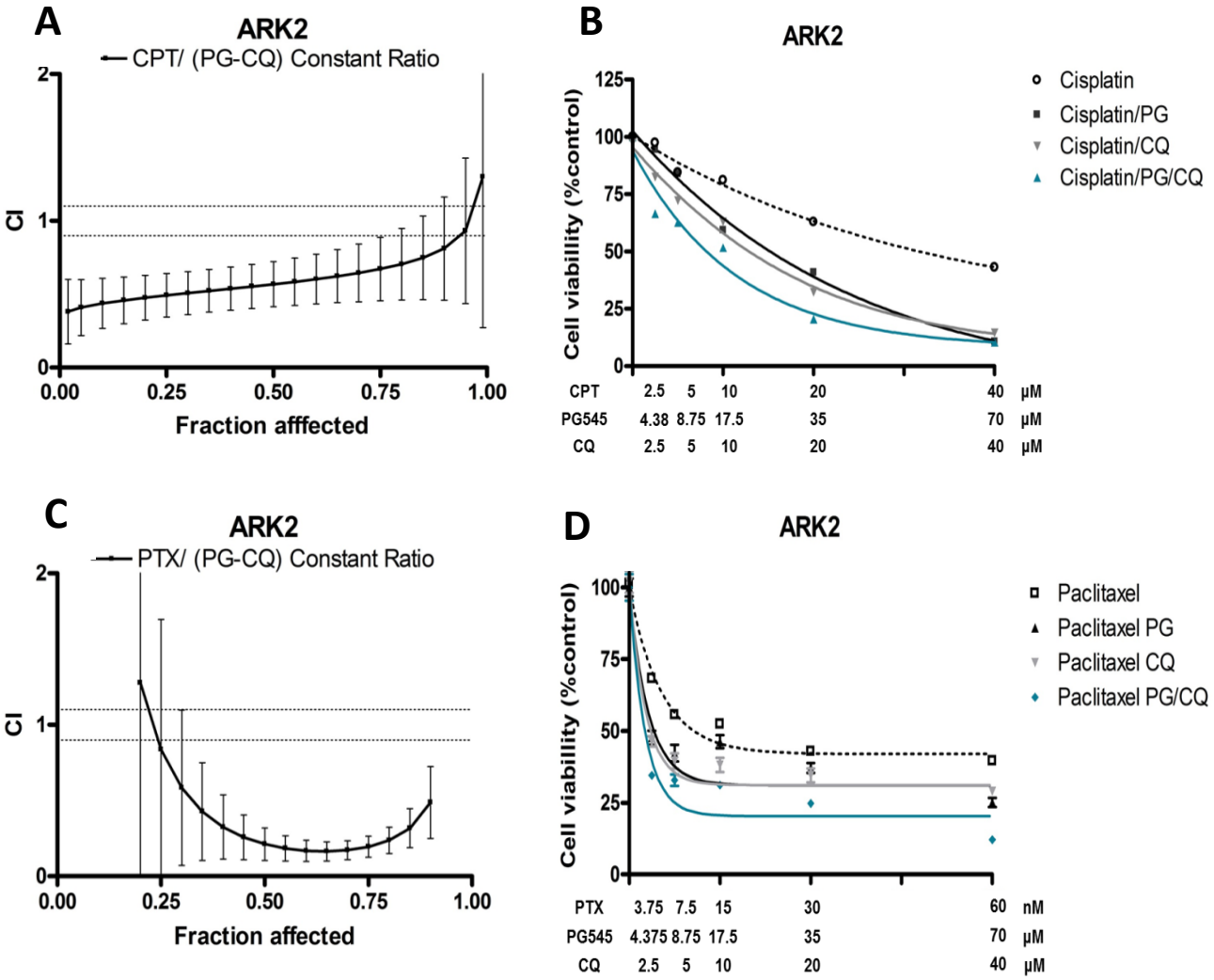

Figure 17: Synergy in a three-drug regimen of PG545, chloroquine and cisplatin or paclitaxel is observed. Combination values between a fixed ratio of PG545 and Chloroquine (70 µM and 40 µM) and cisplatin (CPT) and /or paclitaxel (PTX) were calculated using the Chou Talalay method. Synergy between all three compounds was demonstrated (**A and C**). For illustration purposes cell viability values used for synergy calculation are shown (**B and D**).

4. Discussion

Significant evidence links alterations of the heparanase-heparansulfate-proteoglycan (HSPG)-system to nearly every facet of tumor evolution, including tumorigenesis, progression, metastasis, resistance to chemotherapy, and recurrence [52], [57], [59], [75], [114]. Additionally, individuals with elevated heparanase levels in cancer exhibited a reduced lifespan compared to those with lower heparanase levels [115]. Collectively, these findings propose a general implication of heparanase in the progression of cancer, indicating its potential as a viable target for the development of anticancer drugs. In this study we investigated the effects of the heparan mimetic PG545, a compound targeting the heparanase-HSPG system in endometrial cancer. We demonstrated its effectiveness in both type I and II endometrial cancer uncovering potential avenues how autophagy as cellular response to targeting the HSP-heparanase system may lead to novel combinations of drugs in endometrial cancer.

PG545 is a fully sulfated glycolipid, which has immunomodulatory properties and acts as inhibitor of the heparanase-HSPG system. It has been studied in approximately 30 xenograft and 20 syngeneic models. It is currently undergoing preliminary clinical evaluation under the synonym Pixatimod for its potential application in cancer treatment [116]. To our knowledge this is the first preclinical study to describe the effects of PG545 in endometrial cancer. The therapeutic potential of heparan mimetics, of which PG545 is an example, has garnered increasing attention over the past decade. PG545 is shown to have significant antiproliferative effects in various cancer models [72], [73], [117]. Given the complexity of the heparanase-HSPG-system PG545 acts as multitargeting compound rather than targeting only one very specific genetic alteration in cancers. By binding heparin-binding growth factors (HBGFs), inhibiting heparanase, and impeding growth factor-mediated signaling PG545 is a

promising candidate for addressing the complex biology of a heterogeneous disease such as endometrial cancer. In our study, we demonstrated that PG545 inhibits downstream signaling of HB-GFs in endometrial cancer cells and decreases growth factor mediated migration and invasion in both cell types *in vitro*. PG545 had promising antiproliferative and proapoptotic effects in both type I and type II endometrial cancer cells *in vitro.* Parallel to other cancers PG545 effectively reduced tumor growth in athymic xenograft models and prolonged survival. Clinical markers, including Ki67 and the microvessel density index (iMVD), evaluated through CD31 staining, witnessed marked reductions under PG545 treatment. This suggests a potential inhibition of angiogenesis mediated by FGF2, VEGF, or HB-EGF. These findings underscore the promising therapeutic potential of PG545 in addressing endometrial cancer through its intricate modulation of various key pathways involved in tumorigenesis and angiogenesis.[20], [118]

An additional aspect for therapeutic use of PG545 is its potential to enhance the efficacy of chemotherapeutic regimens [70]. The systemic side effects associated with chemotherapy constitute a significant contributor to morbidity and impact the overall quality of life for cancer patients [10]. Consequently, enhancing the effectiveness of chemotherapy represents an important facet for improving patient outcomes. In alignment with findings observed in various cancer types, our investigations reveal that PG545 demonstrates a synergistic relationship with the chemotherapeutic drugs cisplatin paclitaxel *in vitro* and *in vivo*. In Hec1B cells, recognized as cisplatin-resistant type I cancer cells, as well as ARK2 cells, representative of the more aggressive and typically more chemo resistant type II cancer PG545 sensitized cells to the chemotherapeutic regimen in vitro and prolonged survival of the EC xenografts *in vivo*. Furthermore, the addition of PG545 significantly

amplifies the apoptotic effects induced by cisplatin and paclitaxel in vitro. This dual enhancement of both proliferative and apoptotic responses reinforces the potential of PG545 as a valuable adjunct to conventional chemotherapy.

From a mechanistic standpoint, our study has revealed that the initiation of autophagy in EC cells is prompted by PG545-induced endoplasmic reticulum (ER) stress. The well-established interplay between drug-induced ER stress and the activation of autophagy to maintain ER homeostasis has been extensively reported in scientific literature [117]. Furthermore, PG545 has been demonstrated to block growth factor signaling and induce single- and double-strand DNA breaks, both known triggers of ER stress [69], [119], [120]. By exploring one of the underlying mechanisms of PG545, our findings suggest that PG545 serves as a trigger for autophagy in EC, acting as a defensive mechanism to clear unfolded proteins. This observation aligns with prior research indicating that the inhibition of heparanase-HSPG system can induce ER stress in cancer cells [121]. The concept of autophagy has evolved to be recognized as a double-edged sword [78]. While it traditionally functions as a cellular recycling process that primarily promotes cell survival in nutrient-deficient conditions, its role in cancer cells reveals various forms of autophagy-dependent cell death. Various studies have outlined the different modes of autophagy and apoptosis, emphasizing the coordinated interplay of both processes in parallel [111]. In our specific context, we have demonstrated that PG545, induces ER stress, followed by autophagy as an adaptive response, ultimately culminating in apoptotic cell death. To partially validate our assertion that PG545-induced autophagy is ER stress-dependent, we introduced melatonin, a broad-spectrum ER stress inhibitor. As a result, we observed a reduction in autophagy, substantiated by the decrease in LC3BII. This experimental manipulation further supports our hypothesis regarding the

intricate relationship between PG545, ER stress and autophagy. Similarly, our findings demonstrate that melatonin, an antioxidant and known ER stress inhibitor secreted from the pineal gland, plays a suppressive role in autophagy induced by PG545. Expanding on this, it's noteworthy that a functional inhibitor and close homolog of heparanase-1, namely heparanase-2 (Hpa2), exhibits tumor-suppressive properties by inhibiting heparanase enzymatic activity and fostering ER stress stimulation [122]. Our data highlight that a likely consequence of excess ER stress is cell death since the combination of PG545 with cisplatin in EC cells induces significantly more ER stress *in vitro* compared to treatment of PG545 and/or cisplatin alone.

With PG545 treatment we observed a pronounced induction in autophagy, as indicated by the simultaneous upregulation of LC3BII and downregulation of p62. This underscores that the induction of this intracellular mechanism, akin to the response observed with ER stress, occurs following treatment with PG545 in EC cells. While Shteingautz et al. have demonstrated that PG545 attenuates in HeLa cells, and thereby inhibits growth, our current data contribute to the prevailing understanding that drug-induced autophagy is contingent on context and, more crucially, the specific cell type [75], [79]. Autophagy conventionally serves as a cellular survival mechanism during nutrient deprivation, and typically, the basal level of autophagy tends to be disproportionately elevated compared to normal cells [123]. However, unlike the brief and transient surge in ER stress-induced autophagy, which exerts a cytoprotective role with potential survival benefits, a prolonged and profound ER stress-induced autophagy, surpassing the basal threshold, has the capacity to initiate apoptotic cell death.

In endometrial cancer it appears that autophagy acts as response mechanism of the PG545-induced ER stress. Consequently, the inhibition of autophagy through

chloroquine (CQ) treatment may exacerbate cellular stress by overwhelming cells with an unprocessed protein burden, thereby triggering apoptosis. We demonstrated this by further potentiating the efficacy of PG545 by adding the known autophagy inhibitor chloroquine. We were able to demonstrate that chloroquine sensitizes cells to the effects of PG545. Additionally, it escalates the expression of markers of late apoptosis in cells treated with both compounds. When combined we were able to detect strong synergy between both compounds showing that the cellular response to the heparan mimetic PG545 can be targeted. Additionally, we were able to show that synergy between PG545, chloroquine, cisplatin and paclitaxel persist and are not attenuated when combined. Chloroquine has been demonstrated to independently attenuate chemoresistance in endometrial cancer cells [124]. However, given that PG545 is a multitargeting compound, drug interactions are likely more intricate than demonstrated in our in vitro, single-cell experiments. Therefore, the combination of PG545 with chloroquine and the chemotherapeutic regimen serves as proof of concept and represents an initial step in establishing a multidrug regimen to inhibit autophagy as a response mechanism. Nevertheless, we did not test the other EC cell lines with this combination, hence many more steps both *in vitro* and *in vivo* are necessary to substantiate the benefit of this combination.

To further put the findings of this study in a wider context, we have shown previously that PG545 interferes with Wnt/βcatenin pathway and dislplays antitumor effects in pancreatic cancer cells [73]. This finding reinforces the notion that diminished mitochondrial ATP production and hypoxia contribute to the downregulation of Wnt signaling. This downregulation occurs through the decreased levels of β-catenin, which is a consequence of heightened ER stress. Simultaneously, the hindrance of FGF2 signaling prompts an increase in ER stress within endometrial cancer (EC) cells,

underscoring the intricate interplay between the PG545-induced inhibition of growth factor signaling and the activation of ER stress, subsequently leading to autophagy.

There are important limitations to this study. First, most experiments were only conducted with two cell lines, Hec1B and ARK2 cells. Although we tried to select cells of both type I and type II EC, single cell experiments of both cell lines hardly represent the complex biology of EC. More experiments *in vitro* on i.e. patient-harvested cells may be necessary to determine the effectiveness of PG545. Similar avenues should be explored for further *in vivo* experiments. PG545 demonstrates efficacy in the xenograft model of both type I and II EC. However, the subcutaneous model employed in this study utilizes a monocellular approach, employing only a single distinct cell line per xenograft. Consequently, this model fails to consider intratumoral heterogeneity, thereby reducing its predictive value. Additionally, PG545, which is currently in phase I clinical trials, has a variety of anti-cancer effects and recently also emerged as an immunomodulatory drug (also called Pixatimod), showing potential in activating natural killer cells [67]. Our xenograft models were nude mice, not capable of mobilizing a T cell immune response. The effect of these immunomodulating properties on the progression of endometrial cancer is unclear. Our group showed that PG545 demonstrates similar antiproliferative and chemo enhancing effects in the immunocompetent ovarian cancer xenograft ID8 [70]. Still, studies in Endometrial Cancer are necessary to further determine whether PG545 is a candidate for clinical trials in endometrial cancer. Additionally, autophagy itself is known to have multiple immunomodulatory effects in the microenvironment further complicating the picture [125]. Therefore, it seems reasonable to explore the effects of PG545 in patient-derived xenograft models in the future.

Furthermore, PG545 is a multitargeting compound and we did not describe in this study the impact of PG545 on other signaling pathways known to be altered by PG545. While we outline the effects on HB-EGF and FGF signaling in our investigation, the effects of PG545, as demonstrated in other studies, on other pathways such as the Beta-Catenin pathway, proteoglycans, or extracellular heparinase remain unexplored in EC. As we were focusing on growth factor signaling, we did not explore the heparanase status of the cell lines used. Hence the interplay of PG545 with heparanase is not further described in this study but should play an important role in further investigations. Moreover, the effects of PG545 on chemoresistance warrant further explorations. While the observed chemo sensitizing properties of PG545 are promising, the exact mechanism underlying these properties in Endometrial Cancer nevertheless remains elusive and requires further investigation. Various pathways have been described as mediating chemoresistance in EC, many of which are direct targets of PG545 [11], [34], [75], [126]. Escalating ER stress is a possible mechanism of chemo sensitization with PG545 treatment, and our data adds to this notion. Nevertheless, we did not investigate the effect of ER stress inhibition on chemoresistance and therefore cannot prove that the heightened ER stress observed with the combination of PG545, and cisplatin is responsible for the observed synergistic effects. Similar experimental setups for melatonin, a known ER stress inhibitor, compared to our chloroquine experiments, could provide further guidance on how ER stress inhibitions impacts PG545 and chemo sensitizing properties.

Lastly, *in vitro* and *in vivo* therapeutic markers need to be established to optimize therapeutic regimen containing PG545. IC_{50}-values varied significantly between cell lines in this study. RL95 cells and Ishikawa (IC_{50} = 100 µM) appeared to be more resistant to PG545 than Hec1B (IC_{50} = 70 µM) and ARK2 cells (IC_{50} = 60 µM).

The underlying mechanism for this remains unclear. All four cell lines showed induction of autophagic flux with PG545 treatment, but with different biochemical consequences. We demonstrated that autophagy acts as response-mechanism in EC based on the escalating effects of the chloroquine. Despite the autophagic markers LC3BII and p62 not being rescued in Ishikawa cells when chloroquine was added, we still observed an increase of apoptosis and synergistic effects between PG545 and chloroquine in Ishikawa cells like the other three cell lines. This could be due to several reasons: A suboptimal time point when the lysates were analyzed and effective reduction of autophagic flux had occurred at a different timepoint. Unaccounted off-target interactions between both drugs or a more complex role of autophagy as response mechanism to PG545. Additionally, no reliable in vivo autophagy marker exists, which continues to raise the question whether the effects of PG545 remain *in vivo*. Hence there is a need to further explore response markers *in vitro* and *in vivo*.

In summary, PG545 blocks growth facto-mediated signaling and demonstrates antiproliferative effects in type I and type II EC cells. PG545 synergizes with the chemotherapeutic drugs cisplatin and paclitaxel *in vitro* and *in vivo*. Mechanistically, PG545 induces autophagy as response-mechanism to ER stress. The autophagic response may be exploited as an additional therapeutic target in PG545 treated cells. This is the first study to show PG545's efficacy alone or in combination with chemotherapy in endometrial cancer. These findings support the future exploration of PG545 alone or in combination with chemotherapy in phase I/II clinical trials.

Abstract

Endometrial carcinoma is one of the most common tumors of the female genital tract. Despite advancements in treatment, the prognosis for metastatic endometrial carcinoma remains poor. Current chemotherapeutics often lose clinical efficacy due to the development of chemoresistance during therapy. A potential approach for treating endometrial carcinoma involves the use of "multi-targeting therapies," substances that inhibit multiple biologically relevant signaling pathways. The sulfated glycolipid PG545 is a compound that inhibits several carcinogenic mechanisms and has shown promising antiproliferative effects against various carcinomas.

This study investigates the effects and underlying mechanisms of PG545 application in endometrial carcinoma. It is demonstrated that PG545 inhibits the signaling pathways induced by FGF and HBEGF. Additionally, PG545 exhibits antiproliferative effects in vitro and in vivo against endometrial carcinoma cells. In vitro, PG545 shows strong synergies with the chemotherapeutic agents cisplatin and paclitaxel in both Type I (Hec1B) and Type II (ARK2) cells. Moreover, the combination with cisplatin and paclitaxel results in a significant reduction in tumor mass in xenograft mouse models, ultimately leading to extended survival rates in the combination group compared to the monotherapy arms. This underscores the chemotherapy-enhancing effect of PG545.

Mechanistically, PG545 application induces endoplasmic reticulum stress, subsequently triggering autophagy, a process of cellular homeostasis. The simultaneous increase in autophagy-related proteins, including pERK, Bip/Grp78, IRE1α, Calnexin, and CHOP/GADD153 within 6-24 hours after PG545 administration, supports this observation. The addition of melatonin, known to reduce ER stress, results in a reduction of observed autophagy. Adding chloroquine, an autophagy

inhibitor, further enhances the effect of PG545 without abolishing its synergistic action with cisplatin. This highlights the role of autophagy as a potential rescue mechanism against PG545 and opens up new therapeutic combinations.

Further studies on PG545 and its effects on endometrial carcinoma are needed. Specifically, experiments on patient-derived xenograft mouse models could provide insightful preclinical findings. In summary, it can be demonstrated that PG545 potentiates the effects of the chemotherapeutics cisplatin and paclitaxel in vitro and in vivo in endometrial carcinoma. These findings suggest that PG545 as a combination partner with chemotherapy for endometrial carcinoma holds promise. This presented work is the first study describing the effects of PG545 in endometrial carcinoma. And is previously published in Hoffmann et al., Biochemical Pharmacology, 2020 [80].

Zusammenfassung

Das Endometriumkarzinom zählt zu den häufigsten Tumoren des weiblichen Genitaltraktes. Trotz Fortschritten in der Behandlung ist die Prognose des metastasierten Endometriumkarzinoms schlecht. Aufgrund von sich entwickelnder Chemoresistenz verlieren derzeitige Chemotherapeutika oft klinische Wirksamkeit im Laufe der Therapie. Ein möglicher Ansatz zur Therapie des Endometriumkarzinoms besteht in der Nutzung sogenannter “multi-targeting therapies”, also Wirkstoffen die mehrere biologisch relevante Signalwege inhibieren. Das sulfatierte Glycolipid PG545 ist ein Wirkstoff, der mehrere karzinogene Mechanismen inhibiert. PG545 zeigt vielversprechende antiproliferative Wirkung gegen verschiedene Karzinome. Die vorliegende Arbeit untersucht die Auswirkungen und zugrundeliegenden Mechanismen der Anwendung von PG545 im Endometriumkarzinom. Es kann gezeigt werden, dass PG545 die von FGF und HBEGF induzierten Signalwege hemmt. Außerdem PG545 besitzt antiproliferative Wirkung *in vitro* und *in vivo* gegen Endometriumkarzinomzellen. PG545 zeigt *In vitro* bei sowohl Typ I (Hec1B), als auch Typ II (ARK2) Zellen des Endometriumkarzinoms starke Synergismen mit den klassichen Chemotherapeutika Cisplatin und Paclitaxel, welche die derzeitigen Standardchemotherpaeutika beim Endometriumkarzinom sind. Zudem resultiert die Kombination mit Cisplatin und Paclitaxel in signifikanter Reduzierung an Tumormasse in Xenograft-Mausmodellen und führt letztendlich zu verlängertem Überlebensraten in der Kombinationsgruppe im Vergleich zu den Monotherapiearmen. Dies unterstreicht die Chemotherapie verstärkende Wirkung von PG545. Mechanistisch betrachtet führt PG545-Applikation zu Endoplasmatischen-Retikulum-Stress. Dieser wiederum löst Autophagie, ein Prozess der Zellhomöostase, aus. Gleichzeitiger Anstieg der Autophagie relevanten Proteine pERK, Bip/Grp78, IRE1α, Calnexin und

CHOP/GADD153, innerhalb von 6-24 Stunden nach der Administration von PG545 belegen dies. Durch Hinzugeben von Melatonin, welches bekanntlich ER Stress reduziert, kommt es zu einer Reduzierung von beobachteter Autophagie. Durch Zugabe von Chloroquine, enen Autophhagiehemmer kann die Wirkung von PG545 zusätzlich gesteigert werden ohne die synergistische Wirkung mit Cisplatin aufzuheben. Dies unterstreicht zum einen die Rolle von Autophagie als Rettungsmechanismus gegenüber PG545, zum Anderen ermöglicht es die neue Kombinationen von Therapeutikern. Dennoch bedarf es weiterer Studien zu PG545 und dessen Effekte beim Endometriumkarzinom. Speziell Experimente auf patienten-basierten Xenograft-Mausmodellen könnten aufschlussreiche präklinische Erkenntnisse liefern. Zusammengefasst kann gezeigt werden, dass PG545 die Wirkung von den Chemotherapeutika Cisplatin und Paclitaxel *in vitro* als auch *in vivo* bei Endometriumkarzinom potenziert. Diese Erkenntnisse zeigen, dass PG545 als Kombinationspartner zu klassischer Chemotherapie beim Endometriumkarzinom vielversprechend ist. Die vorgelegte Arbeit beschreibt als erste Studie die Wirkung von PG545 im Endometriumkarzinom.

References

[1] R. Siegel *et al.*, “Cancer treatment and survivorship statistics, 2012,” *CA Cancer J Clin*, vol. 62, no. 4, pp. 220–241, 2012, doi: 10.3322/caac.21149.

[2] S. J. Henley, J. W. Miller, N. F. Dowling, V. B. Benard, and L. C. Richardson, “Uterine Cancer Incidence and Mortality - United States, 1999-2016,” *MMWR Morb Mortal Wkly Rep*, vol. 67, no. 48, pp. 1333–1338, 2018, doi: 10.15585/mmwr.mm6748a1.

[3] R. L. Siegel, K. D. Miller, and A. Jemal, “Cancer statistics, 2020,” *CA Cancer J Clin*, vol. 70, no. 1, pp. 7–30, Jan. 2020, doi: 10.3322/CAAC.21590.

[4] O. Raglan *et al.*, “Risk factors for endometrial cancer: An umbrella review of the literature,” *Int J Cancer*, vol. 145, no. 7, pp. 1719–1730, 2019, doi: 10.1002/ijc.31961.

[5] F. Amant, M. R. Mirza, M. Koskas, and C. L. Creutzberg, “Cancer of the corpus uteri,” *International Journal of Gynecology & Obstetrics*, vol. 143, pp. 37–50, Oct. 2018, doi: 10.1002/ijgo.12612.

[6] W. CREASMAN *et al.*, “Carcinoma of the Corpus Uteri,” *International Journal of Gynecology and Obstetrics*, vol. 95, no. SUPPL. 1, 2006, doi: 10.1016/S0020-7292(06)60031-3.

[7] “Cancer Facts & Figures 2021 | Enhanced Reader.”

[8] N. Colombo *et al.*, “ESMO–ESGO–ESTRO consensus conference on endometrial cancer: Diagnosis, treatment and follow-up,” *Radiotherapy and Oncology*, vol. 117, no. 3, pp. 559–581, Dec. 2015, doi: 10.1016/j.radonc.2015.11.013.

[9] C. M. Bestvina and G. F. Fleming, “Chemotherapy for Endometrial Cancer in Adjuvant and Advanced Disease Settings,” *Oncologist*, vol. 21, no. 10, p. 1250, Oct. 2016, doi: 10.1634/THEONCOLOGIST.2016-0062.

[10] K. Banning *et al.*, “Quality of life in endometrial cancer survivors by grade of disease,” *Cancer Med*, vol. 12, no. 12, p. 13675, Jun. 2023, doi: 10.1002/CAM4.5987.

[11] F. Guo, H. Zhang, Z. Jia, M. Cui, and J. Tian, “Chemoresistance and targeting of growth factors/cytokines signalling pathways: towards the development of effective therapeutic strategy for endometrial cancer.,” *Am J Cancer Res*, vol. 8, no. 7, pp. 1317–1331, 2018, Accessed: Jun. 07, 2020. [Online]. Available: http://www.ncbi.nlm.nih.gov/pubmed/30094104

[12] R. Agarwal and S. B. Kaye, “Ovarian cancer: Strategies for overcoming resistance to chemotherapy,” *Nature Reviews Cancer*, vol. 3, no. 7. European Association for Cardio-Thoracic Surgery, pp. 502–516, 2003. doi: 10.1038/nrc1123.

[13] J. McAlpine, A. Leon-Castillo, and T. Bosse, “The rise of a novel classification system for endometrial carcinoma; integration of molecular subclasses,” *J Pathol*, vol. 244, no. 5, pp. 538–549, 2018, doi: 10.1002/path.5034.

[14] J. V. Bokhman, “Two pathogenetic types of endometrial carcinoma,” *Gynecol Oncol*, vol. 15, no. 1, pp. 10–17, 1983, doi: 10.1016/0090-8258(83)90111-7.

[15] M. J. Carlson, K. W. Thiel, and K. K. Leslie, “Past, present, and future of hormonal therapy in recurrent endometrial cancer,” *Int J Womens Health*, vol. 6, no. 1, p. 429, May 2014, doi: 10.2147/IJWH.S40942.

[16] A. C. Rodriguez, Z. Blanchard, K. A. Maurer, and J. Gertz, “Estrogen Signaling in Endometrial Cancer: a Key Oncogenic Pathway with Several Open Questions,” *Horm Cancer*, vol. 10, no. 2–3, p. 51, Jun. 2019, doi: 10.1007/S12672-019-0358-9.

[17] V. W. Setiawan *et al.*, “Type i and II endometrial cancers: Have they different risk factors?,” *Journal of Clinical Oncology*, vol. 31, no. 20, pp. 2607–2618, Jul. 2013, doi: 10.1200/JCO.2012.48.2596.

[18] D. W. Bell and L. H. Ellenson, “Molecular Genetics of Endometrial Carcinoma,” *https://doi.org/10.1146/annurev-pathol-020117-043609*, vol. 14, pp. 339–367, Jan. 2019, doi: 10.1146/ANNUREV-PATHOL-020117-043609.

[19] J. L. Hecht and G. L. Mutter, “Molecular and pathologic aspects of endometrial carcinogenesis,” *Journal of Clinical Oncology*, vol. 24, no. 29. J Clin Oncol, pp. 4783–4791, Oct. 10, 2006. doi: 10.1200/JCO.2006.06.7173.

[20] N. Bansal, V. Yendluri, and R. M. Wenham, “The molecular biology of endometrial cancers and the implications for pathogenesis, classification, and targeted therapies,” *Cancer Control*, vol. 16, no. 1, pp. 8–13, 2009, doi: 10.1177/107327480901600102.

[21] H. P. Yang *et al.*, “Endometrial Cancer Risk Factors by 2 Main Histologic Subtypes: The NIH-AARP Diet and Health Study,” *Am J Epidemiol*, vol. 177, no. 2, pp. 142–151, Jan. 2013, doi: 10.1093/AJE/KWS200.

[22] T. Okuda *et al.*, “Genetics of Endometrial Cancers,” *Obstet Gynecol Int*, vol. 2010, pp. 1–8, 2010, doi: 10.1155/2010/984013.

[23] A. S. Felix *et al.*, “Associations between hepatocyte growth factor, c-Met, and basic fibroblast growth factor and survival in endometrial cancer patients,” *Br J Cancer*, vol. 106, no. 12, pp. 2004–2009, Jun. 2012, doi: 10.1038/bjc.2012.200.

[24] B. Dobrzycka, B. MacKowiak-Matejczyk, M. Kinalski, and S. J. Terlikowski, “Pretreatment serum levels of bFGF and VEGF and its clinical significance in endometrial carcinoma,” *Gynecol Oncol*, vol. 128, no. 3, pp. 454–460, Mar. 2013, doi: 10.1016/j.ygyno.2012.11.035.

[25] A. A. Kamat *et al.*, “Clinical and biological significance of vascular endothelial growth factor in endometrial cancer,” *Clinical Cancer Research*, vol. 13, no. 24, pp. 7487–7495, Dec. 2007, doi: 10.1158/1078-0432.CCR-07-1017.

[26] G. Scambia *et al.*, “Significance of epidermal growth factor receptor expression in primary human endometrial cancer,” *Int J Cancer*, vol. 56, no. 1, pp. 26–30, 1994, doi: 10.1002/ijc.2910560106.

[27] D. Hanahan, “Hallmarks of Cancer: New Dimensions,” *Cancer Discov*, vol. 12, no. 1, pp. 31–46, Jan. 2022, doi: 10.1158/2159-8290.CD-21-1059.

[28] K. K. Leslie *et al.*, “Tyrosine kinase inhibitors in endometrial cancer,” *International Journal of Gynecological Cancer*, vol. 15, no. 2, pp. 409–411, Mar. 2005, doi: 10.1111/J.1525-1438.2005.ABST_20.X.

[29] T. Mitamura, P. Dong, K. Ihira, M. Kudo, and H. Watari, “Molecular-targeted therapies and precision medicine for endometrial cancer.,” *Jpn J Clin Oncol*, vol. 49, no. 2, pp. 108–120, Feb. 2019, doi: 10.1093/jjco/hyy159.

[30] A. Pavlidou and N. F. Vlahos, “Molecular alterations of PI3K/Akt/mTOR pathway: a therapeutic target in endometrial cancer.,” *ScientificWorldJournal*, vol. 2014, p. 709736, 2014, doi: 10.1155/2014/709736.

[31] C. Kandoth *et al.*, “Integrated genomic characterization of endometrial carcinoma,” *Nature*, vol. 497, no. 7447, pp. 67–73, 2013, doi: 10.1038/nature12113.

[32] V. Gagnon, I. Mathieu, É. Sexton, K. Leblanc, and E. Asselin, “AKT involvement in cisplatin chemoresistance of human uterine cancer cells,” *Gynecol Oncol*, vol. 94, no. 3, pp. 785–795, Sep. 2004, doi: 10.1016/j.ygyno.2004.06.023.

[33] F. Fabi, P. Adam, S. Parent, L. Tardif, M. Cadrin, and E. Asselin, “Pharmacologic inhibition of Akt in combination with chemotherapeutic agents effectively induces apoptosis in ovarian and endometrial cancer cell lines,” *Mol Oncol*, vol. 15, no. 8, p. 2106, Aug. 2021, doi: 10.1002/1878-0261.12888.

[34] J. Girouard, M. J. Lafleur, S. Parent, V. Leblanc, and E. Asselin, “Involvement of Akt isoforms in chemoresistance of endometrial carcinoma cells,” *Gynecol Oncol*, vol. 128, no. 2, pp. 335–343, Feb. 2013, doi: 10.1016/J.YGYNO.2012.11.016.

[35] V. Gagnon, C. Van Themsche, S. Turner, V. Leblanc, and E. Asselin, “Akt and XIAP regulate the sensitivity of human uterine cancer cells to cisplatin, doxorubicin and taxol,” *Apoptosis*, vol. 13, no. 2, pp. 259–271, Feb. 2008, doi: 10.1007/S10495-007-0165-6.

[36] M. C. Mendoza, E. E. Er, and J. Blenis, “The Ras-ERK and PI3K-mTOR pathways: Cross-talk and compensation,” *Trends in Biochemical Sciences*, vol. 36, no. 6. NIH Public Access, pp. 320–328, Jun. 2011. doi: 10.1016/j.tibs.2011.03.006.

[37] Y. Sun *et al.*, “Down-regulation of RIP3 potentiates cisplatin chemoresistance by triggering HSP90-ERK pathway mediated DNA repair in esophageal squamous cell carcinoma,” *Cancer Lett*, vol. 418, pp. 97–108, Apr. 2018, doi: 10.1016/j.canlet.2018.01.022.

[38] J. W. Zhou, J. J. Tang, W. Sun, and H. Wang, “PGK1 facilities cisplatin chemoresistance by triggering HSP90/ERK pathway mediated DNA repair and methylation in endometrial endometrioid adenocarcinoma,” *Mol Med*, vol. 25, no. 1, Mar. 2019, doi: 10.1186/S10020-019-0079-0.

[39] M. Villedieu, E. Deslandes, M. Duval, J. F. Héron, P. Gauduchon, and L. Poulain, “Acquisition of chemoresistance following discontinuous exposures to cisplatin is associated in ovarian carcinoma cells with progressive alteration of FAK, ERK and p38 activation in response to treatment,” *Gynecol Oncol*, vol. 101, no. 3, pp. 507–519, Jun. 2006, doi: 10.1016/j.ygyno.2005.11.017.

[40] S. Lheureux *et al.*, “Moving forward with actionable therapeutic targets and opportunities in endometrial cancer: A NCI clinical trials planning meeting report,” *Gynecol Oncol*, vol. 149, no. 3, pp. 442–446, Jun. 2018, doi: 10.1016/j.ygyno.2018.02.005.

[41] Q. B. She, D. B. Solit, Q. Ye, K. E. O’Reilly, J. Lobo, and N. Rosen, “The BAD protein integrates survival signaling by EGFR/MAPK and PI3K/Akt kinase pathways in PTEN-deficient tumor cells,” *Cancer Cell*, vol. 8, no. 4, pp. 287–297, Oct. 2005, doi: 10.1016/j.ccr.2005.09.006.

[42] J. A. Engelman *et al.*, “Effective use of PI3K and MEK inhibitors to treat mutant Kras G12D and PIK3CA H1047R murine lung cancers,” *Nat Med*, vol. 14, no. 12, pp. 1351–1356, Dec. 2008, doi: 10.1038/nm.1890.

[43] M. K. Halle *et al.*, “HER2 expression patterns in paired primary and metastatic endometrial cancer lesions.,” *Br J Cancer*, vol. 118, no. 3, pp. 378–387, Feb. 2018, doi: 10.1038/bjc.2017.422.

[44] V. Castonguay *et al.*, “A phase II trial of sunitinib in women with metastatic or recurrent endometrial carcinoma: A study of the Princess Margaret, Chicago and California Consortia,” *Gynecol Oncol*, vol. 134, no. 2, pp. 274–280, 2014, doi: 10.1016/j.ygyno.2014.05.016.

[45] K. K. Leslie *et al.*, “A phase II evaluation of gefitinib in the treatment of persistent or recurrent endometrial cancer: A Gynecologic Oncology Group study,” *Gynecol Oncol*, vol. 129, no. 3, pp. 486–494, Jun. 2013, doi: 10.1016/j.ygyno.2013.02.019.

[46] A. N. Fader *et al.*, “Randomized Phase II Trial of Carboplatin-Paclitaxel Versus Carboplatin-Paclitaxel-Trastuzumab in Uterine Serous Carcinomas That Overexpress Human Epidermal Growth Factor Receptor 2/neu,” *J Clin Oncol*, vol. 36, no. 20, pp. 2044–2051, Jul. 2018, doi: 10.1200/JCO.2017.76.5966.

[47] A. N. Fader *et al.*, “Randomized Phase II Trial of Carboplatin-Paclitaxel Compared with Carboplatin-Paclitaxel-Trastuzumab in Advanced (Stage III-IV) or Recurrent Uterine Serous Carcinomas that Overexpress Her2/Neu (NCT01367002): Updated Overall Survival Analysis,” *Clin Cancer Res*, vol. 26, no. 15, pp. 3928–3935, Aug. 2020, doi: 10.1158/1078-0432.CCR-20-0953.

[48] D. Bender *et al.*, “A phase II evaluation of cediranib in the treatment of recurrent or persistent endometrial cancer: An NRG Oncology/Gynecologic Oncology Group study,” in *Gynecologic Oncology*, Academic Press Inc., Sep. 2015, pp. 507–512. doi: 10.1016/j.ygyno.2015.07.018.

[49] A. Papa, E. Zaccarelli, D. Caruso, P. Vici, P. Benedetti Panici, and F. Tomao, “Targeting angiogenesis in endometrial cancer - New agents for tailored treatments,”

Expert Opinion on Investigational Drugs, vol. 25, no. 1. Taylor and Francis Ltd, pp. 31–49, Jan. 02, 2016. doi: 10.1517/13543784.2016.1116517.

[50] S. Sarrazin, W. C. Lamanna, and J. D. Esko, “Heparan Sulfate Proteoglycans,” *Cold Spring Harb Perspect Biol*, vol. 3, no. 7, pp. 1–33, 2011, doi: 10.1101/CSHPERSPECT.A004952.

[51] R. Sasisekharan, Z. Shriver, G. Venkataraman, and U. Narayanasami, “Roles of heparan-sulphate glycosaminoglycans in cancer,” *Nat Rev Cancer*, vol. 2, no. 7, pp. 521–528, Jul. 2002, doi: 10.1038/nrc842.

[52] I. Vlodavsky *et al.*, “Heparanase: From basic research to therapeutic applications in cancer and inflammation,” *Drug Resist Updat*, vol. 29, pp. 54–75, 2016, doi: 10.1016/j.drup.2016.10.001.

[53] Z. Xiong *et al.*, “Downregulation of heparanase by RNA interference inhibits invasion and tumorigenesis of hepatocellular cancer cells in vitro and in vivo.,” *Int J Oncol*, vol. 40, no. 5, pp. 1601–9, May 2012, doi: 10.3892/ijo.2012.1338.

[54] I. Vlodavsky and Y. Friedmann, “Molecular properties and involvement of heparanase in cancer metastasis and angiogenesis,” *Journal of Clinical Investigation*, vol. 108, no. 3. The American Society for Clinical Investigation, pp. 341–347, 2001. doi: 10.1172/JCI13662.

[55] D. R. Coombe and N. S. Gandhi, “Heparanase: A Challenging Cancer Drug Target,” *Frontiers in Oncology*, vol. 9. Frontiers Media S.A., p. 1316, Nov. 28, 2019. doi: 10.3389/fonc.2019.01316.

[56] V. C. Ramani, P. S. Pruett, C. A. Thompson, L. D. DeLucas, and R. D. Sanderson, “Heparan sulfate chains of syndecan-1 regulate ectodomain shedding,” *Journal of Biological Chemistry*, vol. 287, no. 13, pp. 9952–9961, Mar. 2012, doi: 10.1074/jbc.M111.330803.

[57] O. Jung *et al.*, “Heparanase-induced shedding of syndecan-1/CD138 in myeloma and endothelial cells activates VEGFR2 and an invasive phenotype: prevention by novel synstatins,” *Oncogenesis*, vol. 5, no. 2, pp. e202–e202, Feb. 2016, doi: 10.1038/oncsis.2016.5.

[58] Y. Yang *et al.*, “Nuclear heparanase-1 activity suppresses melanoma progression via its DNA-binding affinity,” *Oncogene*, vol. 34, no. 47, pp. 5832–5842, Nov. 2015, doi: 10.1038/onc.2015.40.

[59] J. Canaani, N. Ilan, S. Back, G. Gutman, I. Vlodavsky, and D. Grisaru, “Heparanase expression increases throughout the endometrial hyperplasia-cancer sequence,” 2007, doi: 10.1016/j.ijgo.2007.10.019.

[60] J. Kodama *et al.*, “Heparanase expression in both normal endometrium and endometrial cancer,” *International Journal of Gynecologic Cancer*, vol. 16, no. 3, pp. 1401–1406, Apr. 2006, doi: 10.1136/ijgc-00009577-200605000-00069.

[61] M. Inamine *et al.*, “Heparanase expression in endometrial cancer: analysis of immunohistochemistry,” *J Obstet Gynaecol*, vol. 28, no. 6, pp. 634–637, 2008, doi: 10.1080/01443610802323542.

[62] M. Kato, S. Saunders, H. Nguyen, and M. Bernfield, “Loss of cell surface syndecan-1 causes epithelia to transform into anchorage-independent mesenchyme-like cells.,” *https://doi.org/10.1091/mbc.6.5.559*, vol. 6, no. 5, pp. 559–576, Oct. 2017, doi: 10.1091/MBC.6.5.559.

[63] J. Roche, “The Epithelial-to-Mesenchymal Transition in Cancer,” *Cancers (Basel)*, vol. 10, no. 2, p. 52, Feb. 2018, doi: 10.3390/CANCERS10020052.

[64] J. H. Oh, H. S. Lee, S. H. Park, H. S. Ryu, and C. K. Min, “Syndecan-1 overexpression promotes tumor growth and angiogenesis in an endometrial cancer xenograft model,” *International Journal of Gynecological Cancer*, vol. 20, no. 5, pp. 751–756, Jul. 2010, doi: 10.1111/IGC.0b013e3181e02faa.

[65] K. M. Jayatilleke and M. D. Hulett, “Heparanase and the hallmarks of cancer,” *Journal of Translational Medicine 2020 18:1*, vol. 18, no. 1, pp. 1–25, Nov. 2020, doi: 10.1186/S12967-020-02624-1.

[66] E. Hammond, P. Handley, K. Dredge, and I. Bytheway, “Mechanisms of heparanase inhibition by the heparan sulfate mimetic PG545 and three structural analogues,” *FEBS Open Bio*, vol. 3, pp. 346–351, 2013, doi: 10.1016/j.fob.2013.07.007.

[67] K. Dredge *et al.*, “A Phase i study of the novel immunomodulatory agent PG545 (pixatimod) in subjects with advanced solid tumours,” *Br J Cancer*, vol. 118, no. 8, pp. 1035–1041, Apr. 2018, doi: 10.1038/s41416-018-0006-0.

[68] K. Dredge *et al.*, “The PG500 series: Novel heparan sulfate mimetics as potent angiogenesis and heparanase inhibitors for cancer therapy,” *Invest New Drugs*, vol. 28, no. 3, pp. 276–283, Jun. 2010, doi: 10.1007/s10637-009-9245-5.

[69] V. Ferro *et al.*, “Discovery of PG545: a highly potent and simultaneous inhibitor of angiogenesis, tumor growth, and metastasis,” *J Med Chem*, vol. 55, no. 8, pp. 3804–3813, 2012, doi: 10.1021/jm201708h.

[70] B. Winterhoff *et al.*, “PG545 enhances anti-cancer activity of chemotherapy in ovarian models and increases surrogate biomarkers such as VEGF in preclinical and clinical plasma samples,” *Eur J Cancer*, vol. 51, no. 7, pp. 879–892, 2015, doi: 10.1016/j.ejca.2015.02.007.

[71] U. Ray *et al.*, “PG545 sensitizes ovarian cancer cells to PARP inhibitors through modulation of RAD51-DEK interaction,” *Oncogene 2023 42:37*, vol. 42, no. 37, pp. 2725–2736, Aug. 2023, doi: 10.1038/s41388-023-02785-5.

[72] K. T. Ostapoff *et al.*, “PG545, an Angiogenesis and Heparanase Inhibitor, Reduces Primary Tumor Growth and Metastasis in Experimental Pancreatic Cancer,” *Mol Cancer Ther*, vol. 12, no. 7, pp. 1190–1201, 2013, doi: 10.1158/1535-7163.MCT-12-1123.

[73] D. B. Jung *et al.*, “The heparan sulfate mimetic PG545 interferes with Wnt/beta-catenin signaling and significantly suppresses pancreatic tumorigenesis alone and in combination with gemcitabine,” *Oncotarget*, vol. 6, no. 7, pp. 4992–5004, 2015, doi: 10.18632/oncotarget.3214.

[74] T. V Brennan *et al.*, “Heparan sulfate mimetic PG545-mediated antilymphoma effects require TLR9-dependent NK cell activation,” *J Clin Invest*, vol. 126, no. 1, pp. 207–219, 2016, doi: 10.1172/JCI76566.

[75] A. Shteingauz *et al.*, “Heparanase Enhances Tumor Growth and Chemoresistance by Promoting Autophagy,” *Cancer Res*, vol. 75, no. 18, pp. 3946–3957, 2015, doi: 10.1158/0008-5472.CAN-15-0037.

[76] R. Khandia *et al.*, “A Comprehensive Review of Autophagy and Its Various Roles in Infectious, Non-Infectious, and Lifestyle Diseases: Current Knowledge and Prospects for Disease Prevention, Novel Drug Design, and Therapy,” *Cells*, vol. 8, no. 7, p. 674, Jul. 2019, doi: 10.3390/CELLS8070674.

[77] J. M. Mulcahy Levy and A. Thorburn, “Autophagy in cancer: moving from understanding mechanism to improving therapy responses in patients,” *Cell Death & Differentiation 2019 27:3*, vol. 27, no. 3, pp. 843–857, Dec. 2019, doi: 10.1038/s41418-019-0474-7.

[78] R. Chavez-Dominguez, M. Perez-Medina, J. S. Lopez-Gonzalez, M. Galicia-Velasco, and D. Aguilar-Cazares, “The Double-Edge Sword of Autophagy in Cancer: From Tumor Suppression to Pro-tumor Activity,” *Front Oncol*, vol. 10, p. 578418, Oct. 2020, doi: 10.3389/FONC.2020.578418.

[79] B. Linder and D. Kögel, “Autophagy in Cancer Cell Death,” *Biology (Basel)*, vol. 8, no. 4, Dec. 2019, doi: 10.3390/BIOLOGY8040082.

[80] R. Hoffmann *et al.*, “Sulfated glycolipid PG545 induces endoplasmic reticulum stress and augments autophagic flux by enhancing anticancer chemotherapy efficacy in endometrial cancer,” *Biochem Pharmacol*, vol. 178, Aug. 2020, doi: 10.1016/j.bcp.2020.114003.

[81] S. A. Mullany *et al.*, “Expression and functional significance of HtrA1 loss in endometrial cancer,” *Clin Cancer Res*, vol. 17, no. 3, pp. 427–436, 2011, doi: 10.1158/1078-0432.CCR-09-3069.

[82] M. Nishida, “The Ishikawa cells from birth to the present,” *Hum Cell*, vol. 15, no. 3, pp. 104–117, 2002, doi: 10.1111/J.1749-0774.2002.TB00105.X.

[83] R. Pavlič *et al.*, “In the Model Cell Lines of Moderately and Poorly Differentiated Endometrial Carcinoma, Estrogens Can Be Formed via the Sulfatase Pathway,” *Front Mol Biosci*, vol. 8, p. 743403, Nov. 2021, doi: 10.3389/FMOLB.2021.743403/BIBTEX.

[84] H. Kurarmoto, M. Hamano, and M. Imai, “HEC-1 cells,” *Hum Cell*, vol. 15, no. 2, pp. 81–95, 2002, doi: 10.1111/J.1749-0774.2002.TB00103.X.

[85] J. G. Bosquet *et al.*, “Association of a novel endometrial cancer biomarker panel with prognostic risk, platinum insensitivity, and targetable therapeutic options,” *PLoS One*, vol. 16, no. 1, Jan. 2021, doi: 10.1371/JOURNAL.PONE.0245664.

[86] A. Takahashi *et al.*, “Metformin impairs growth of endometrial cancer cells via cell cycle arrest and concomitant autophagy and apoptosis,” *Cancer Cell Int*, vol. 14, no. 1, p. 53, Jun. 2014, doi: 10.1186/1475-2867-14-53.

[87] E. Kalogera *et al.*, “Quinacrine in endometrial cancer: Repurposing an old antimalarial drug,” *Gynecol Oncol*, vol. 146, no. 1, pp. 187–195, 2017, doi: 10.1016/j.ygyno.2017.04.022.

[88] T. C. Chou, “Drug combination studies and their synergy quantification using the Chou-Talalay method,” *Cancer Res*, vol. 70, no. 2, pp. 440–446, 2010, doi: 10.1158/0008-5472.CAN-09-1947.

[89] A. Khurana *et al.*, “Quinacrine promotes autophagic cell death and chemosensitivity in ovarian cancer and attenuates tumor growth,” *Oncotarget*, vol. 6, no. 34, pp. 36354–36369, 2015, doi: 10.18632/oncotarget.5632.

[90] A. Al-Najar *et al.*, “Microvessel density as a prognostic factor in penile squamous cell carcinoma,” *Urologic Oncology: Seminars and Original Investigations*, vol. 30, no. 3, pp. 325–329, May 2012, doi: 10.1016/j.urolonc.2010.03.016.

[91] V. J. Tuominen, S. Ruotoistenmäki, A. Viitanen, M. Jumppanen, and J. Isola, “ImmunoRatio: A publicly available web application for quantitative image analysis of estrogen receptor (ER), progesterone receptor (PR), and Ki-67,” *Breast Cancer Research*, vol. 12, no. 4, pp. 1–12, Jul. 2010, doi: 10.1186/BCR2615/FIGURES/7.

[92] S. Guo *et al.*, “A rapid and high content assay that measures cyto-ID-stained autophagic compartments and estimates autophagy flux with potential clinical applications,” *Autophagy*, vol. 11, no. 3, p. 560, Jan. 2015, doi: 10.1080/15548627.2015.1017181.

[93] D. Roy *et al.*, “Loss of HSulf-1: The Missing Link between Autophagy and Lipid Droplets in Ovarian Cancer,” *Scientific Reports 2017 7:1*, vol. 7, no. 1, pp. 1–13, Feb. 2017, doi: 10.1038/srep41977.

[94] C. Mauvezin and T. P. Neufeld, “Bafilomycin A1 disrupts autophagic flux by inhibiting both V-ATPase-dependent acidification and Ca-P60A/SERCA-dependent autophagosome-lysosome fusion,” *Autophagy*, vol. 11, no. 8, pp. 1437–1438, Jan. 2015, doi: 10.1080/15548627.2015.1066957.

[95] S. Sarkar Bhattacharya, C. Mandal, R. S. Albiez, S. K. Samanta, and C. Mandal, “Mahanine drives pancreatic adenocarcinoma cells into endoplasmic reticular stress-mediated apoptosis through modulating sialylation process and Ca2+-signaling,” *Sci Rep*, vol. 8, no. 1, Dec. 2018, doi: 10.1038/s41598-018-22143-w.

[96] M. Dowsett *et al.*, “Assessment of Ki67 in Breast Cancer: Recommendations from the International Ki67 in Breast Cancer Working Group,” *JNCI Journal of the National Cancer Institute*, vol. 103, no. 22, p. 1656, Nov. 2011, doi: 10.1093/JNCI/DJR393.

[97] L. L. Y. Chan *et al.*, “A novel image-based cytometry method for autophagy detection in living cells,” *Autophagy*, vol. 8, no. 9, pp. 1371–1382, 2012, doi: 10.4161/auto.21028.

[98] T. Farkas, M. Høyer-Hansen, and M. Jäättelä, “Identification of novel autophagy regulators by a luciferase-based assay for the kinetics of autophagic flux,” *Autophagy*, vol. 5, no. 7, pp. 1018–1025, Oct. 2009, doi: 10.4161/auto.5.7.9443.

[99] D. J. Klionsky *et al.*, “Guidelines for the use and interpretation of assays for monitoring autophagy in higher eukaryotes,” *Autophagy*, vol. 4, no. 2. Taylor and Francis Inc., pp. 151–175, Feb. 16, 2008. doi: 10.4161/auto.5338.

[100] S. Kim, S. Choi, and D. Kang, “Quantitative and qualitative analysis of autophagy flux using imaging,” *BMB Rep*, vol. 53, no. 5, p. 241, May 2020, doi: 10.5483/BMBREP.2020.53.5.046.

[101] S. Chipurupalli, U. Samavedam, and N. Robinson, “Crosstalk Between ER Stress, Autophagy and Inflammation,” *Front Med (Lausanne)*, vol. 8, p. 758311, Nov. 2021, doi: 10.3389/FMED.2021.758311/BIBTEX.

[102] X. Fu *et al.*, “Endoplasmic reticulum stress, cell death and tumor: Association between endoplasmic reticulum stress and the apoptosis pathway in tumors (Review),” *Oncol Rep*, vol. 45, no. 3, pp. 801–808, Mar. 2021, doi: 10.3892/OR.2021.7933/HTML.

[103] M. Ogata *et al.*, “Autophagy is activated for cell survival after endoplasmic reticulum stress,” *Mol Cell Biol*, vol. 26, no. 24, pp. 9220–9231, 2006, doi: 10.1128/MCB.01453-06.

[104] T. Yorimitsu, U. Nair, Z. Yang, and D. J. Klionsky, “Endoplasmic reticulum stress triggers autophagy,” *J Biol Chem*, vol. 281, no. 40, pp. 30299–30304, 2006, doi: 10.1074/jbc.M607007200.

[105] M. Cnop, S. Toivonen, M. Igoillo-Esteve, and P. Salpea, “Endoplasmic reticulum stress and eIF2α phosphorylation: The Achilles heel of pancreatic β cells,” *Mol Metab*, vol. 6, no. 9, p. 1024, Sep. 2017, doi: 10.1016/J.MOLMET.2017.06.001.

[106] C. J. Adams, M. C. Kopp, N. Larburu, P. R. Nowak, and M. M. U. Ali, “Structure and molecular mechanism of ER stress signaling by the unfolded protein response signal activator IRE1,” *Front Mol Biosci*, vol. 6, no. MAR, p. 439177, Mar. 2019, doi: 10.3389/FMOLB.2019.00011/BIBTEX.

[107] H. Nishitoh, “CHOP is a multifunctional transcription factor in the ER stress response,” *J Biochem*, vol. 151, no. 3, pp. 217–219, Mar. 2012, doi: 10.1093/JB/MVR143.

[108] M. Wang, S. Wey, Y. Zhang, R. Ye, and A. S. Lee, “Role of the Unfolded Protein Response Regulator GRP78/BiP in Development, Cancer, and Neurological Disorders,” *Antioxid Redox Signal*, vol. 11, no. 9, p. 2307, Sep. 2009, doi: 10.1089/ARS.2009.2485.

[109] R. Guérin, G. Arseneault, S. Dumont, and L. A. Rokeach, “Calnexin is involved in apoptosis induced by endoplasmic reticulum stress in the fission yeast,” *Mol Biol Cell*, vol. 19, no. 10, pp. 4404–4420, Oct. 2008, doi: 10.1091/mbc.E08-02-0188.

[110] C. Fan *et al.*, “Melatonin suppresses ER stress-dependent proapoptotic effects via AMPK in bone mesenchymal stem cells during mitochondrial oxidative damage,” *Stem Cell Res Ther*, vol. 11, no. 1, pp. 1–22, Dec. 2020, doi: 10.1186/S13287-020-01948-5/FIGURES/9.

[111] D. Denton and S. Kumar, “Autophagy-dependent cell death,” *Cell Death Differ*, vol. 26, no. 4, pp. 605–616, 2019, doi: 10.1038/s41418-018-0252-y.

[112] B. Zhang *et al.*, “The tumor therapy landscape of synthetic lethality,” *Nature Communications 2021 12:1*, vol. 12, no. 1, pp. 1–11, Feb. 2021, doi: 10.1038/s41467-021-21544-2.

[113] J. Foucquier and M. Guedj, “Analysis of drug combinations: current methodological landscape,” *Pharmacol Res Perspect*, vol. 3, no. 3, Jun. 2015, doi: 10.1002/PRP2.149.

[114] I. Vlodavsky *et al.*, “Significance of heparanase in cancer and inflammation,” *Cancer Microenviron*, vol. 5, no. 2, pp. 115–132, 2012, doi: 10.1007/s12307-011-0082-7.

[115] T. Zahavi *et al.*, “Heparanase: a potential marker of worse prognosis in estrogen receptor-positive breast cancer,” *npj Breast Cancer 2021 7:1*, vol. 7, no. 1, pp. 1–9, May 2021, doi: 10.1038/s41523-021-00277-x.

[116] E. Hammond and K. Dredge, “Heparanase Inhibition by Pixatimod (PG545): Basic Aspects and Future Perspectives,” *Adv Exp Med Biol*, vol. 1221, pp. 539–565, 2020, doi: 10.1007/978-3-030-34521-1_22.

[117] K. Dredge *et al.*, “PG545, a dual heparanase and angiogenesis inhibitor, induces potent anti-tumour and anti-metastatic efficacy in preclinical models,” *Br J Cancer*, vol. 104, no. 4, pp. 635–642, 2011, doi: 10.1038/bjc.2011.11.

[118] S. A. Byron and P. M. Pollock, “FGFR2 as a molecular target in endometrial cancer,” *Future Oncology*, vol. 5, no. 1, pp. 27–32, 2009, doi: 10.2217/14796694.5.1.27.

[119] E. Dufey *et al.*, “Genotoxic stress triggers the activation of IRE1α-dependent RNA decay to modulate the DNA damage response,” *Nature Communications 2020 11:1*, vol. 11, no. 1, pp. 1–13, May 2020, doi: 10.1038/s41467-020-15694-y.

[120] U. Ray *et al.*, “PG545 sensitizes ovarian cancer cells to PARP inhibitors through modulation of RAD51-DEK interaction,” *Oncogene 2023 42:37*, vol. 42, no. 37, pp. 2725–2736, Aug. 2023, doi: 10.1038/s41388-023-02785-5.

[121] I. Vlodavsky, M. Gross-Cohen, M. Weissmann, N. Ilan, and R. D. Sanderson, “Opposing Functions of Heparanase-1 and Heparanase-2 in Cancer Progression,” *Trends Biochem Sci*, vol. 43, no. 1, pp. 18–31, 2018, doi: 10.1016/j.tibs.2017.10.007.

[122] I. Vlodavsky, Y. Kayal, M. Hilwi, S. Soboh, R. D. Sanderson, and N. Ilan, “Heparanase—A single protein with multiple enzymatic and nonenzymatic functions,” *Proteoglycan Research*, vol. 1, no. 3, p. e6, Jul. 2023, doi: 10.1002/PGR2.6.

[123] M. Wang, M. E. Law, R. K. Castellano, and B. K. Law, “The unfolded protein response as a target for anticancer therapeutics,” *Crit Rev Oncol Hematol*, vol. 127, pp. 66–79, 2018, doi: 10.1016/j.critrevonc.2018.05.003.

[124] T. Fukuda *et al.*, “The anti-malarial chloroquine suppresses proliferation and overcomes cisplatin resistance of endometrial cancer cells via autophagy inhibition,” *Gynecol Oncol*, vol. 137, no. 3, pp. 538–545, Jun. 2015, doi: 10.1016/J.YGYNO.2015.03.053.

[125] D. J. Puleston and A. K. Simon, “Autophagy in the immune system,” *Immunology*, vol. 141, no. 1, pp. 1–8, Jan. 2014, doi: 10.1111/imm.12165.

[126] K. Brasseur, N. Gévry, and E. Asselin, “Chemoresistance and targeted therapies in ovarian and endometrial cancers,” *Oncotarget*, vol. 8, no. 3, pp. 4008–4042, Dec. 2017, doi: 10.18632/oncotarget.14021.

Acknowledgments

First, I would like to thank my in-laboratory supervisor Professor Shridhar at Mayo Clinic. Furthermore, I would like to thank Prof. Dr. Schmidmaier for his supervision and guidance for all these years during this project and making it possible to conduct this thesis. My gratitude also goes to my co-workers Dr. Sayantani Bhattacharya and Dr. Roy Debarshi, who taught me all laboratory techniques mentioned in this manuscript. I express my thankfulness to Dr. Boris Winterhoff, who connected me with Professor Shridhar and her working group. Thank you to Keith Dredge and Edward Hammond for their knowledgeable input regarding the effects of PG545. We acknowledge Prof. Shi-Wen Jiang and Prof. Karl C. Podratz, (Mayo Clinic, Rochester, MN) for ARK2 cell line and Dr. Paul Goodfellow (Washington University, St. Louis, MO) for kindly providing us the Ishikawa and RL95 cell lines.

Grant Support- This work was supported by the Department of Laboratory Medicine and Pathology, (VS), Mayo Clinic, Rochester.

Affidavit

LMU LUDWIG-MAXIMILIANS-UNIVERSITÄT MÜNCHEN | Promotionsbüro Medizinische Fakultät | MMRS

Affidavit

Hoffmann, Robert Maximilian

Surname, first name

Street

Zip code, town, country

I hereby declare, that the submitted thesis entitled:

The effects of the heparan mimetic PG545 on cell growth and chemoresistance in Endometrial Cancer.

is my own work. I have only used the sources indicated and have not made unauthorized use of services of a third party. Where the work of others has been quoted or reproduced, the source is always given.

I further declare that the dissertation presented here has not been submitted in the same or similar form to any other institution for the purpose of obtaining an academic degree.

Munich, 12.7.2024 — Robert Maximilian Hoffmann

place, date — Signature doctoral candidate

Curriculum Vitae (aus Datenschutzgründen entfernt)

Publikationsliste

1. **Robert M. Hoffmann**, MD,Mark Neuman MD, MPH, Michelle Du BS, Michael C. Monuteaux, ScD, Andrew F. Miller, MD, Jeffrey T. Neal, MD, Kyle A. Nelson, MD[1,], Cynthia A Gravel, MD. Lung Ultrasound in the Evaluation of Asthma Exacerbation in Children and Adolescents. (submitted)

2. **Hoffmann RM**, Neal JT, Arichai P, Gravel CA, Neuman MI, Monuteaux MC, Levy JA, Miller AF. Test Characteristics of Cardiac Point-of-Care Ultrasound in Children With Preexisting Cardiac Conditions. Pediatr Emerg Care. 2023 Sep 7. doi: 10.1097/PEC.0000000000003050. Epub ahead of print. PMID: 37678275.
3. Rosen RH, Epee-Bounya A, Curran D, Chung S, **Hoffmann R**, Lee LK, Marcus C, Mateo CM, Miller JE, Nereim C, Silberholz E, Shah SN, Theodoris CV, Wardell H, Winn AS, Toomey S, Finkelstein JA, Ward VL, Starmer A; BOSTON CHILDREN'S HOSPITAL RACE, ETHNICITY, AND ANCESTRY IN CLINICAL PATHWAYS WORKING GROUP. Race, Ethnicity, and Ancestry in Clinical Pathways: A Framework for Evaluation. Pediatrics. 2023 Nov 17:e2022060730. doi: 10.1542/peds.2022-060730. Epub ahead of print. PMID: 37974460.

4. **Hoffmann RM,** Miller AF. A review of the 2020 update of the Pediatric Advanced Life Support guidelines. Pediatr Emerg Med Pract. 2023 Jun 1;20(6):1-28. PMID: 37207313.

5. **Hoffmann RM,** Miller K. Adherent foreign body on the uvula. Ann Emerg Med. 2022 Jul;80(1):21-45. doi: 10.1016/j.annemergmed.2022.01.010. PMID: 35717112.

6. Bechard LJ, Earthman CP, Farr B, Ariagno KA, **Hoffmann RM,** Pham IV, Mehta NM. Feasibility of bioimpedance spectroscopy and long-term functional assessment in critically ill children. Clin Nutr ESPEN. 2022 Feb;47:405-409. doi: 10.1016/j.clnesp.2021.12.009. Epub 2021 Dec 13. PMID: 35063234.

7. Wasserman MG, **Hoffmann RM.** To Err in Medicine: A Trainee-Centered Approach to Medical Mistakes. Acad Med. 2022 Jul 1;97(7):953. doi: 10.1097/ACM.0000000000004421. Epub 2022 Jun 23. PMID: 34554951.

8. **Hoffmann RM,** Ariagno KA, Pham IV, Barnewolt CE, Jarrett DY, Mehta NM, Kantor DB. Ultrasound Assessment of Quadriceps Femoris Muscle Thickness

in Critically Ill Children. Pediatr Crit Care Med. 2021 Oct 1;22(10):889-897. doi: 10.1097/PCC.0000000000002747. PMID: 34028373.

9. Bechard L, Earthman C, Farr B, Ariagno K, **Hoffmann R,** Pham I, Mehta N. Bioimpedance Spectroscopy in Critically Ill Children – Feasibility and Association with Protein Intake and Functional Status. Curr Dev Nutr. 2020 May 29;4(Suppl 2):1118. doi: 10.1093/cdn/nzaa055_003. PMCID: PMC7259036.

10. **Hoffmann R,** Sarkar Bhattacharya S, Roy D, Winterhoff B, Schmidmaier R, Dredge K, Hammond E, Shridhar V. Sulfated glycolipid PG545 induces endoplasmic reticulum stress and augments autophagic flux by enhancing anticancer chemotherapy efficacy in endometrial cancer. Biochem Pharmacol. 2020 Aug;178:114003. doi: 10.1016/j.bcp.2020.114003. Epub 2020 Apr 28. PMID: 32360360; PMCID: PMC8048055.

11. Roy D, Mondal S, Khurana A, Jung DB, **Hoffmann R,** He X, Kalogera E, Dierks T, Hammond E, Dredge K, Shridhar V. Loss of HSulf-1: The Missing Link between Autophagy and Lipid Droplets in Ovarian Cancer. Sci Rep. 2017 Feb 7;7:41977. doi: 10.1038/srep41977. PMID: 28169314; PMCID: PMC5294412.

12. Winterhoff B, Freyer L, Hammond E, Giri S, Mondal S, Roy D, Teoman A, Mullany SA, **Hoffmann R,** von Bismarck A, Chien J, Block MS, Millward M, Bampton D, Dredge K, Shridhar V. PG545 enhances anti-cancer activity of chemotherapy in ovarian models and increases surrogate biomarkers such as VEGF in preclinical and clinical plasma samples. Eur J Cancer. 2015 May;51(7):879-892. doi: 10.1016/j.ejca.2015.02.007. Epub 2015 Mar 5. PMID: 25754234; PMCID: PMC4402130.

13. Roy D, Mondal S, Wang C, He X, Khurana A, Giri S, **Hoffmann R,** Jung DB, Kim SH, Chini EN, Periera JC, Folmes CD, Mariani A, Dowdy SC, Bakkum-Gamez JN, Riska SM, Oberg AL, Karoly ED, Bell LN, Chien J, Shridhar V. Loss of HSulf-1 promotes altered lipid metabolism in ovarian cancer. Cancer Metab. 2014 Aug 18;2:13. doi: 10.1186/2049-3002-2-13. Erratum in: Cancer Metab. 2014;2:24. PMID: 25225614; PMCID: PMC4164348.